Tree Physiology, 2024, **44**, tpae041
https://doi.org/10.1093/treephys/tpae041
Research paper

Wet canopy photosynthesis in a temperate Japanese cypress forest

Linjie Jiao[1,2,*], **Yoshiko Kosugi**[1], **Ayaka Sakabe**[1,3], **Yuichi Sempuku**[1,4], **Ting-Wei Chang**[5], **Siyu Chen**[1]

[1]Forest Hydrology Laboratory, Division of Forest and Biomaterials Science, Graduate School of Agriculture, Kyoto University, Kyoto 606-8502, Japan
[2]Key Laboratory of Tropical Forest Ecology, Xishuangbanna Tropical Botanical Garden, Chinese Academy of Sciences, Menglun 666303, China
[3]Hakubi Center for Advanced Research, Kyoto University, Kyoto 606-8501, Japan
[4]East Nippon Expressway Company Ltd. Kanto Branch, Chiba, Management Office Chiba, Chiba 263-0001, Japan
[5]Laboratory of Plant and Environmental Sciences, School of Food and Nutritional Sciences, University of Shizuoka,52-1 Yada, Suruga-Ku, Shizuoka 422-8526, Japan

*Corresponding author. Key Laboratory of Tropical Forest Ecology, Xishuangbanna Tropical Botanical Garden, Chinese Academy of Sciences, Menglun 666303, China. Email: jiaolinj@gmail.com

Handling Editor: David Whitehead

This study aimed to reveal the mechanism and significance of wet canopy photosynthesis during and after rainfall in temperate coniferous ecosystems by evaluating the influence of abaxial leaf interception on wet canopy photosynthesis. We used the eddy covariance method in conjunction with an enclosed-path gas analyser to conduct continuous ecosystem CO_2 flux observations in a Japanese cypress forest within the temperate Asian monsoon area over 3 years. The observation shows that wet-canopy CO_2 uptake predominantly occurred during the post-rainfall canopy-wet period rather than the during-rainfall period. Then, the measured canopy-wet net ecosystem exchange was compared with the soil–vegetation–atmosphere transfer multilayer model simulations under different parameter settings of the abaxial (lower) leaf surface wet area ratio. The multilayer model predicted net ecosystem exchange most accurately when it assumed the wet area ratio of the abaxial surface was 50% both during and after rainfall. For the wet canopy both during and after rainfall, the model overestimated CO_2 uptake when it assumed no abaxial interception in the simulation, but underestimated CO_2 uptake when it assumed that the entire abaxial leaf surface was wet. These results suggest that the abaxial surface of the Japanese cypress leaf is only partly wet to maintain stomatal openness and a low level of photosynthesis. These results allow for an evaluation of the effect of rainfall on forest carbon circulation under a changing climate, facilitating an improvement of ecosystem carbon exchange models.

Key words: CO_2 flux, eddy covariance, leaf wetness, rainfall, soil respiration.

Introduction

Forests are widely regarded as carbon sinks of the utmost importance. Long-term ecosystem flux observations have improved our understanding of carbon exchange regulation in forest ecosystems across different contexts, including different moisture conditions (Baldocchi et al. 2001; Amiro et al. 2006; Saigusa et al. 2008; Ueyama et al. 2011; Fei et al. 2018). Canopies, across different biomes, can be wet for different periods (Dawson and Goldsmith 2018). For example, they can be wet for <2 h (i.e. in arid regions) to >14 h per day (i.e. in wet regions) (Binks et al. 2021). Although temperate forests are not as frequently wet as tropical forests, they have been shown to be wet for 147 days per year (Dawson and Goldsmith 2018). However, compared with dry canopies, the carbon exchange of the wet canopies has been shown to be less. Nowadays, the application of an enclosed-path gas analyser in an eddy covariance (EC) system can help us achieve a direct and stable measurement of CO_2 flux from the wet forest canopy during and after rainfall (Burba et al. 2010); its application in this study allowed us to assess wet leaf photosynthesis at the canopy (ecosystem) level. A notable accumulated CO_2 uptake was observed in the wet canopy of Japanese cypress (Jiao et al. 2021) when applying this method. In addition, a smaller average net ecosystem exchange (NEE) was observed in the dry canopy than in the wet canopy in a temperate Japanese cypress forest (Sempuku et al. 2018; Jiao et al. 2021). However, the mechanisms and parameters underlying the occurrence of wet-canopy photosynthesis remain unclear.

The slow diffusion of CO_2 through water (Nobel 1991) leads to a reduction in the photosynthetic rate of wet leaves, which is considered to be the main reason for depressed photosynthesis in wet leaves (Ishibashi and Terashima 1995; Chu et al. 2014). Meanwhile, photosynthesis is depressed more when the side of the leaf (abaxial or adaxial) with higher stomatal density is wet (Kimura and Tanakamaru 1981; Hanba et al. 2004). However, compared with the artificial misting experiment, the abaxial surface of the hypo-stomatal species may not be wetted during natural rainfall events, especially for species with flat and horizontally oriented leaves (Berry and Goldsmith 2020). Clarifying interception by the abaxial side of leaves and the extent to which the abaxial surface gets wet is important for understanding the broad-scale processes shaping the occurrence of photosynthesis in a wet canopy consisting of hypo-stomatous species. Through a combination of simulations via the soil–vegetation–atmosphere transfer (SVAT) multilayer model and EC measurements of canopy evapotranspiration, Jiao et al. (2022) were able to determine

Received: March 31, 2023. **Accepted:** April 3, 2024

the extent to which abaxial interception contributed to evapotranspiration for Japanese cypress during and after rainfall. While wet canopy evapotranspiration was largely contributed by interception evaporation, the discussion relating to stomatal activities (i.e. transpiration and photosynthesis) during the canopy-wet period was largely restricted in that study. Therefore, analysing the CO_2 flux (F_c) of the wet canopy in different abaxial side interception situations can help improve our understanding of stomatal activity during the canopy-wet period and its influence on wet canopy CO_2 exchange.

Soil respiration is another important process that contributes the most to temperate evergreen forest CO_2 flux (Curiel Yuste et al. 2004; Davidson et al. 2006; Song et al. 2013) besides photosynthesis, and is one of the dominant components of CO_2 flux measured by the EC method. Rainfall also influences soil respiration. Soil respiration stimulated by rain pulses, which cannot be explained by the relationship between soil moisture and temperature, has been observed at many sites (Lee et al. 2002; Baldocchi and Xu 2007; Sakabe et al. 2015). This means that in traditional soil respiration models that rely on temperature change (e.g. Q_{10} model and Arrhenius model (Fang and Moncrieff 2001)) are hard to precisely predict the change in soil respiration during and after rainfall. Therefore, to evaluate canopy photosynthesis and the long-term forest carbon sink function, it is also important to correctly evaluate the change in soil respiration related to rainfall and account for its influence on F_c simulation.

Based on the results that Japanese cypress canopies can maintain CO_2 uptake during wetting events (Sempuku et al. 2018; Jiao et al. 2021, 2022), we hypothesize that photosynthesis by wet canopies is due to the incomplete wetting of the abaxial leaf surfaces. The present study extends the previous work of Jiao et al. (2022), which modelled the effect of canopy water interception on NEE while testing for the effect of partial abaxial leaf wetness on NEE. To do this, it is necessary to improve the representation of soil respiration in the existing SVAT model. Thus, this study aims to (i) characterize the effect of rain events on soil respiration; and (ii) test whether wet-canopy NEE was best represented by 0%, 50% or 100% interception wetness of the abaxial leaf surfaces.

Materials and methods

Site description

From October 2016 to December 2019, we observed ecosystem fluxes of CO_2 and H_2O and canopy (leaf) wetness in Kiryu Experimental Watershed (site code KEW in AsiaFlux, 34°58′N, 135°59′E) in Shiga Prefecture, Japan. The main plant at this site is Japanese cypress (*Chamaecyparis obtuse* Sieb. Et Zucc.), a commonly planted evergreen coniferous species in the Asian monsoon region. Japanese cypress was planted around 1959 in this watershed and has not been actively managed, so the forest is generally an even-aged stand with little structural heterogeneity composed of thin and spindly trees (Katsuyama et al. 2021). Japanese cypress has flat and scaled leaves, which are unlike the needle leaves of other conifers. The Y-band stomates of the Japanese cypress are distributed only on the abaxial surface of its scale leaves (Pariyar et al. 2017; Kim 2018) (Fig. 1). Therefore, Japanese cypress leaves may maintain gas exchange if no water film or droplets block stomata on the abaxial side of the leaves. The top of the canopy is 20 m above ground level. The average diameter at breast height and tree height is 20.9 cm and 17.8 m, and the basal area is 56.6 m^2 ha^{-1} in 2017.

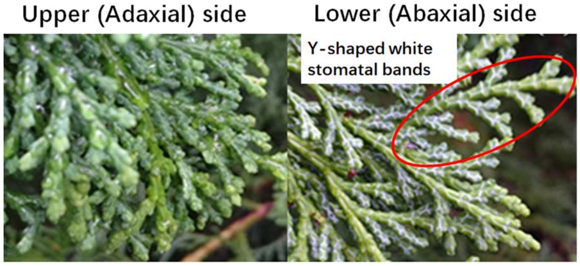

Figure 1. Distribution of stomata on the abaxial and adaxial sides of Japanese cypress leaves.

The meteorological tower for the EC and canopy meteorology measurements is located at one of the catchments in the watershed. The average annual precipitation from 2016 to 2019 was 1785 mm. A total of 39.6% of days in a year were rainy days on average. The average rainfall duration on rainy days is 3.6 h from 2016 to 2019. The frequency of the rainfall events that resulted in constant wetting events during the experimental period, 63.8%, 21.4% and 14.8%, of which were 0 to 5 mm/12 h (small rainfall), 5 to 15 mm/12 h (middle rainfall), and over 15 mm/12 h (heavy rainfall), respectively (Jiao et al. 2022). Fog rarely occurred at this temperate site.

Eddy covariance and meteorological measurements

The flux fetch area was 750 m in the northwest direction and over 2000 m in the other directions. Daytime winds are mainly from the north or west, and nighttime winds are mainly from the south in all seasons. The EC system was placed at the top of the tower (29 m above the ground) and included a 3D anemometer (SAT550, Kaijo, Japan) and an enclosed CO_2/H_2O analyser (LI7200, LI-COR, USA). An enclosed-path gas analyser is capable of precisely measuring ecosystem fluxes during and after rainfall (Aubinet 2008). The sampling frequency and flow rate of the enclosed gas analyser were 10 Hz and 10 L min^{-1}, respectively. Approximately 92% of flux in the daytime and 81% of flux in the nighttime from the footprint was contributed by the forest in the study area (Takanashi et al. 2005; Kosugi et al. 2007). Although EC sites often exhibit the problem of increased data loss at night due to low winds, thermal stratification and turbulence (Burba 2013), this study only used the daytime data (08:00 to 16:00) to analyse wet canopy photosynthesis. Therefore, the EC fluxes are capable to represent the diurnal gas exchange between the forest and air. Flux Calculator software (Ueyama et al. 2012) was used to perform flux calculations and corrections. After removing spikes, crosswind and water vapour corrections to the sensible heat flux, double rotation (McMillen 1988; Wilczak et al. 2001), high-frequency loss correction, lag-time correction and instationary tests (Foken and Wichura 1996) were completed after collecting the raw data. The time lags for H_2O and CO_2 were determined when there was a maximum covariance between the vertical wind velocity and the CO_2/H_2O mole fraction for the enclosed-path system. The relationship between the normalized co-spectrum of the sensible heat flux (H_s) and F_c and the frequency of the enclosed gas analyser under dry and wet conditions was calculated and showed an agreement. This enclosed-path system does not require the Webb, Pearman and Leuning (WPL) correction (Webb and Leuning 1980) for the effect of air density fluctuations because it outputs true dry mole fractions at high speeds (Nakai et al. 2011; Burba 2013). Rainfall can also induce potential measurement errors in sonic anemometers (e.g. obstacles in the path and droplets on transducers) (van Boxel et al. 2004; Zhang et al. 2016), which can be calibrated using the Flux Calculator in de-spike, quality control and gap-filling procedures. This study used a 30-min averaging interval of CO_2 flux to match the chamber measurement of soil respiration. NEE was calculated from F_c and CO_2 storage fluxes (S_c). S_c was estimated from the change in CO_2 concentration measured by the LI7200. The NEE gap-filling and S_c estimation procedures have been described in a previous study at the KEW site (Kosugi et al. 2013). A negative NEE indicates a net CO_2 uptake from the atmosphere to the ecosystem. The same set of 15-min interval λE data from Jiao et al. (2022) was used to better match the changes in rainfall and canopy wetness. The final λE was corrected with sensible heat flux, net radiation, and soil heat flux using the Bowen ratio to achieve an energy balance. Validation of the 15-min interval and energy balance of the same set of data was reported by Jiao et al. (2022).

Two pyranometers (CMP6 Albedometer Kit, Kipp & Zonen, The Netherlands) and 2 long-wave radiometers (CGR, Kipp & Zonen) were used to measure the downward and upward radiation at the top of the tower. A platinum thermometer and capacitive relative humidity sensor (HMP45AC, Vaisala, Finland) set in ventilated radiation-shielded cylinders were used to measure the air temperature and relative humidity. The gross rainfall at this site was measured using a heated tipping bucket rain gauge (RT-5E, Ikeda, Japan) at an open-screen site in the watershed. CR10 data logger was used to collect meteorological data. The meteorological and EC data used in this study were collected from October 2016 to December 2019.

Soil respiration measurement and gap-filling

Soil respiration (R_s) was continuously measured in 30-min interval using automated chambers at three plots near the tower (Sakabe et al. 2015; Makita et al. 2018). The distance between each plot was >25 m. At each plot, the copper-constantan thermocouples were used to measure the soil temperatures at a depth of 2 cm, and three water content reflectometers (CS615 or CS616; Campbell Scientific, USA) were used to measure the soil moisture levels at a depth of 0–30 cm. There was 40% of data missing on R_s during the experimental period owing to the automated chamber malfunctions and site electricity problems. Among them, 16% of the R_s data were missing on rainy days. A random forest (RF) model (sklearn.ensemble.RandomForestRegressor) based on the Scikit-learn library of Python (version 3.6) was applied to predict the missing R_s data in the three plots using soil temperature, soil water content and rainfall data. The advantage of the RF model is that it can predict non-normal distributed data and non-linearly relationships without assuming the data distribution. Considering the influence of rainfall pulses on R_s, we used the RF model to predict missing data on rainy and dry days, respectively. The RF model builds a number of decision trees with controlled variances using bagging (Breiman 2001). First, every decision tree in the RF was generated to classify the target variable, R_s, using the feature variables (soil temperature, soil water content and rainfall amount) with samples that were chosen at random. The selection of features is used to construct each decision tree for classification and regression as well as random sampling of the complete dataset. Random selection without replacement was then used for all features. The training subset selected from the total dataset comprises approximately two-thirds of the dataset. The remaining out-of-bag data were used to assess the effectiveness of the decision tree and significance of the dataset that was not included in the training subset. Each decision tree in a group of decision trees contributes to the final prediction in ensemble learning; averaging the findings of all the separate trees yielded the final expected value. We applied the RF model to R_s regression with 1000 decision trees using rainy- and dry-day datasets, respectively.

The multilayer model applies Q_{10} model to the R_s sub-model (Kosugi et al. 2006, Appendix A.7). Q_{10} model and its parameter space are defined as follows:

$$R_s = R_{sref} Q_{10}^{\frac{T_{soil} - T_{ref}}{10}} \quad (1)$$

where T_{soil} and T_{ref} are observed soil temperature and referenced temperature; R_s and R_{sref} are the respiration rates (μmol m^{-2} s^{-1}) at T_{soil} and T_{ref}, respectively. In this study, T_{ref} is 15 °C. R_{sref} and Q_{10} were obtained by Curve Fitting Toolbox of MATLAB R2014a (MathWorks, Natick, MA, USA), using the observed R_s and soil temperature.

The prediction of Q_{10} model was checked using the observed R_s to avoid the influence of rainy-day R_s in the final ecosystem F_c simulation. If the Q_{10} model could not accurately predict R_s (especially during and after rainfall), the simulated R_s was replaced by the average gap-filled observed R_s weighted by the area of the three plots.

Leaf and canopy wetness

Leaf wetness was measured using a type of handmade resistance-based wetness sensor (Takanashi et al. 2003; Jiao et al. 2021) (Fig. 2a) and was defined as the free water on the leaf surface in this study (Magarey et al. 2005; Park et al. 2019). The output signal of the leaf wetness sensor was recorded by CR10 data logger (Fig. 2b). Sensor signals change when leaf wetness results in a change in sensor resistance and variation in voltage. The sensors were set at the top, middle, and bottom leaf layers of the canopy (19.4, 18.6 and 17.4 m above the ground) (Fig. 2c). Ten sensors were attached to different leaves by random selection in each leaf layer from 2016 to 10 August 2018. The number of sensors in the top and bottom leaf layers was adjusted to 8 and 6, respectively, after 10 August 2018 because of the malfunction of the logger channels. The sensors were only set on the adaxial leaf surface because the sensors on the abaxial side were easily bent during typhoons. Part of the canopy with attached sensors was also within the dominant fetch of the EC measurements. The canopy is defined as 'wet' when there was at least one sensor responding to the wetness, and the canopy is defined as 'dry' only when all the sensors had no response. After dividing the canopy-wet and canopy-dry periods according to the wetness sensor data, we classified the canopy-wet period to 'wet during rainfall' and 'wet after rainfall'. According to the rainfall amount that results in a wetness event (continuous wetness without dry time), 'wet after rainfall' was divided into 'wet after small rainfall', 'wet after middle rainfall', and 'wet after heavy rainfall'. The

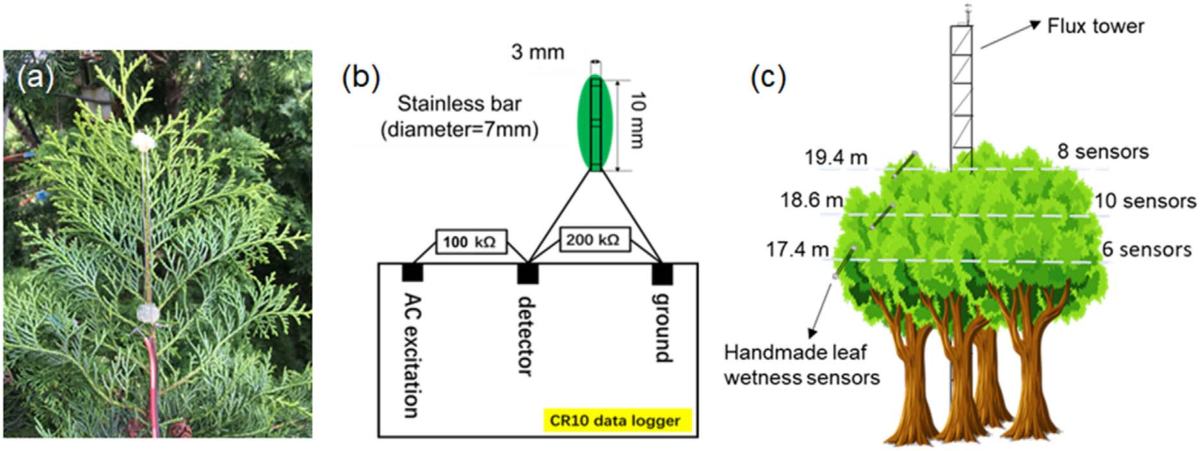

Figure 2. Connection and placement of leaf wetness sensors. (a) A leaf wetness sensor attached to a randomly selected leaf. (b) Connection between leaf wetness sensor and CR10 data logger. (c) Leaf wetness sensors' placements and numbers in the canopy.

intensities of small, medium and heavy rainfall events were defined as 0 to 5 mm/12 h, 5 to 15 mm/12 h and >15 mm/12 h, respectively.

SVAT multilayer model

We used a SVAT multilayer model for CO_2 and H_2O exchange in the C3 plant community (Tanaka 2002; Kosugi et al. 2006). The SVAT multilayer model used in this study was formed by the following sub-models: (i) Reynolds stress, sensible heat exchange, and CO_2 and H_2O exchanges of leaves and the ground surface (Appendix A.1); (ii) stomatal conductance and net photosynthesis in individual leaves (Appendix A.2); (iii) radiative transfer within and above the canopy (Appendix A.3); (iv) the energy balance of leaves and the ground surface (Appendix A.4); (v) atmospheric diffusion within and above the canopy (Appendix A.5); (vi) the rainfall interception and the water budget of leaves (Appendix A.6); and (vii) soil respiration (Appendix A.7). Appendix A.8 shows the parameter for F_c simulation. Based on the original multilayer model (Tanaka 2002; Kosugi et al. 2006), H_2O and CO_2 fluxes in different interception situations can be simulated by modifying the sub-model of rainfall interception and the leaf water budget. The canopy was divided into 100 layers to prevent leaf clumping in each layer, according to Baldocchi and Hutchison (1986). Besides comparing the average of simulated and measured flux, we apply the mean absolute error (MAE), root mean square error (RMSE), and coefficient of determination (R^2) to evaluate the model precision, which can be estimated as follows:

$$MAE = \frac{1}{n}\sum_{i=1}^{n}\left(x_{sim} - x_{obs}\right) \tag{2}$$

$$RMSE = \sqrt{\frac{1}{n}\sum_{i=1}^{n}\left(x_{sim} - x_{obs}\right)^2} \tag{3}$$

$$R^2 = 1 - \frac{\sum_{i=1}^{n}\left(x_{sim} - x_{obs}\right)^2}{\sum_{i=1}^{n}\left(x_{obs} - x_{avg}\right)^2} \tag{4}$$

Sub-models of interception and leaf water balance

To verify the hypothesis that the abaxial side of the leaves in Japanese cypress canopy is not completely wet during and after rainfall to maintain photosynthesis, four models with different interception solutions were applied in this study, based on the original SVAT model (Fig. 3). All four models exhibited interception on the entire surface of the adaxial side and the same leaf water storage capacity on the adaxial side. In Model 1, the abaxial leaf surface cannot be wetted by interception; in Model 2, for per leaf area, only 50% area of the abaxial leaf surface can be wetted during and after rainfall, and another half of abaxial surface remains dry, and the wetted area of the abaxial and the adaxial sides have same leaf water storage capacity; in Model 3, the whole area of the abaxial leaf surface can be completely wetted during and after rainfall, whereas the leaf water storage capacity of the wetted area on the abaxial side is half of that on the adaxial side; and in Model 4, the whole abaxial leaf surface can be wetted during and after rainfall, and it has the same leaf water storage capacity as the adaxial surface did. Therefore, theoretically, the abaxial surfaces in Model 1 only get slightly wet when condensation (the amount of which is much smaller than interception) happens; at least half of the abaxial surfaces keep dry in Model 2 situation; while Models 3 and 4 can achieve the situation that all the abaxial surfaces in the canopy get wet after enough rainfall. Models 1 and 4 are the conditions used for λE simulation in Jiao et al. (2022). The parameters listed in Appendix A.8 are fixed across all four models used in this study. A brief sensitivity analyses of the leaf sensible heat transfer coefficient (C_b, Eqs A.10 and A.11), stomatal coefficient (m, Eq. A.25), and upper leaf water storage capacity (W_{Umax}, Eqs A.64, A.68 and A.71) are presented in Appendix A.9; these analyses were conducted because these three parameters are crucial for the estimation of water transfer and photosynthesis in the wet canopy. In this study, W_{Umax} was a fixed value obtained in a previous study via a leaf-wetting experiment (Jiao et al. 2022). Table 1 shows a set of parameters that mainly differentiate the four models (see Appendix A.6). Based on these four different interception situations, this study will compare the relationship between net radiation (R_n, which is the energy source of evapotranspiration, and represents the level of solar radiation) and simulated and observed NEE, compare the simulated and observed λE, and evaluate the seasonal change of canopy-wet period NEE during rainfall and after different levels of rainfall in comparison with the canopy-dry period.

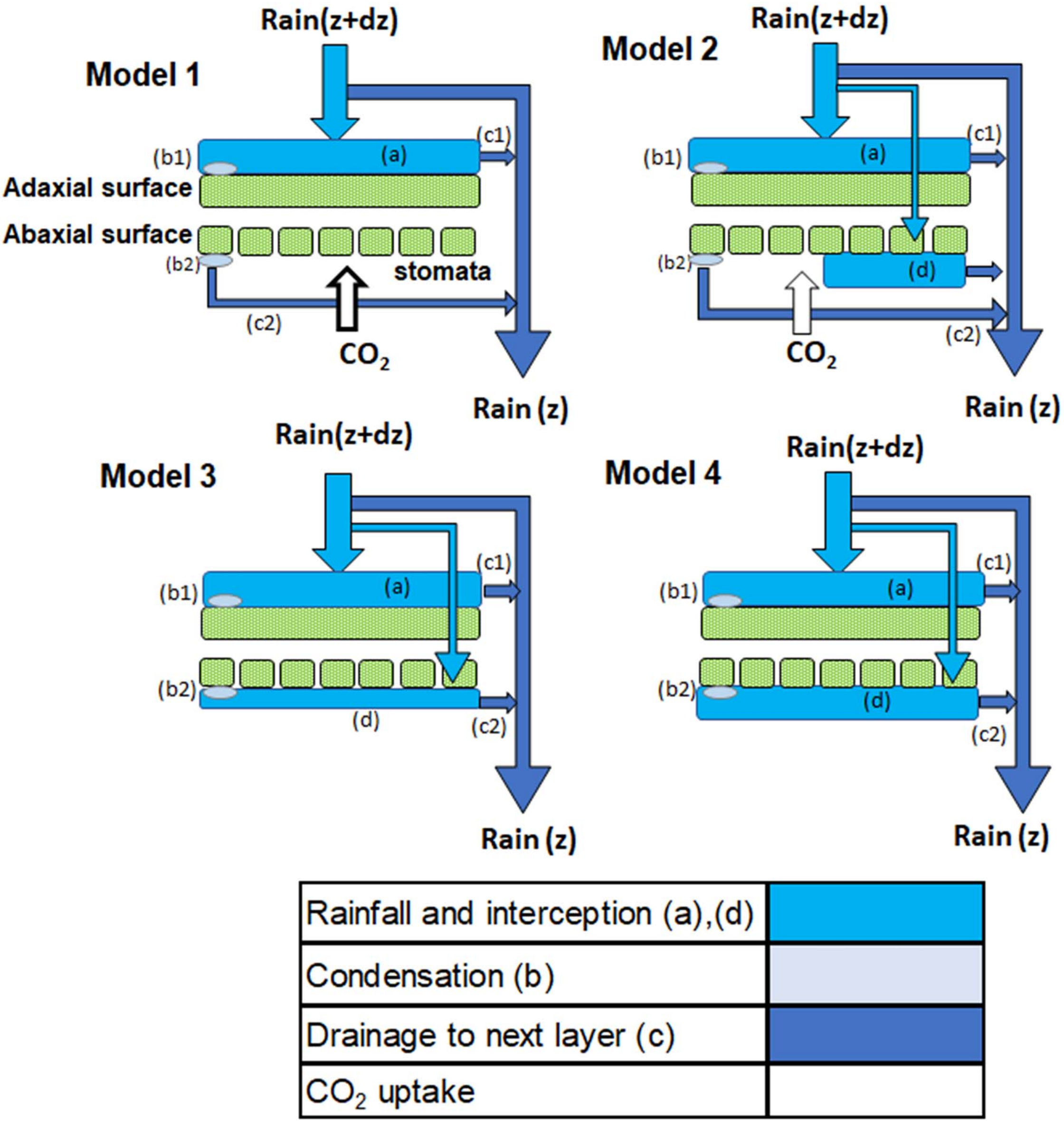

Figure 3. Conceptual figure of the interception subroutine (interception process in per leaf area) Models 1–4, respectively. Rain (z): rainfall and drainage from the upper layer that passed to layer z; (a): the interception by the adaxial side of leaves; (b1): condensation on the adaxial surface of leaves; (b2): condensation on the abaxial surface of leaves; (c1): the drainage water from the adaxial leaf wetness to the next layer, which is resulted from the abaxial condensation and interception in both Models 1 and 4; (c2): the drainage water from the abaxial surface to the next layer, which is resulted from abaxial condensation in Model 1, and the sum of abaxial condensation and interception in Models 2, 3, 4; (d): the interception by the abaxial side of leaves that only happens in Models 2, 3, 4.

Table 1. Key parameters that differ across the four models.

	Abaxial interception capacity (P_L)	Maximum abaxial wet area ratio (r_{wetL})	Maximum abaxial leaf water storage (W_{Lmax}, mm per unit leaf area)
Model 1	0	1	0.18
Model 2	1	0.5	0.18
Model 3	1	1	0.09
Model 4	1	1	0.18

Results

Soil CO_2 flux

In the context of soil temperature, data points of higher R_s were observed more during the canopy-wet period than during the canopy-dry period (Fig. 4). This study used Q_{10} model when the reference soil temperature was 15 °C; however, this did not allow for accurate predictions of R_s spikes during the canopy-wet period. At the annual and half-week scales, RF model brought forth predictions that were more accurate than those of the Q_{10} model (Fig. 5). R^2 of the RF

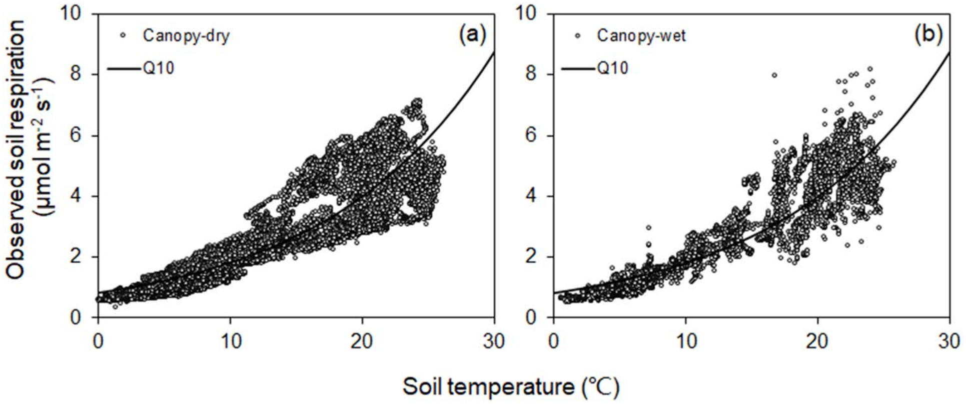

Figure 4. Relationship between soil temperature and the area-weighted average soil CO_2 flux of the 3 plots near flux tower measured by the automated chamber. (a) Observed and Q_{10}-simulated soil CO_2 flux during dry periods in the canopy. (b) Observed and Q_{10}-simulated soil CO_2 flux at during wet periods in the canopy. The Q10 model is applied when the reference temperature is 15 °C.

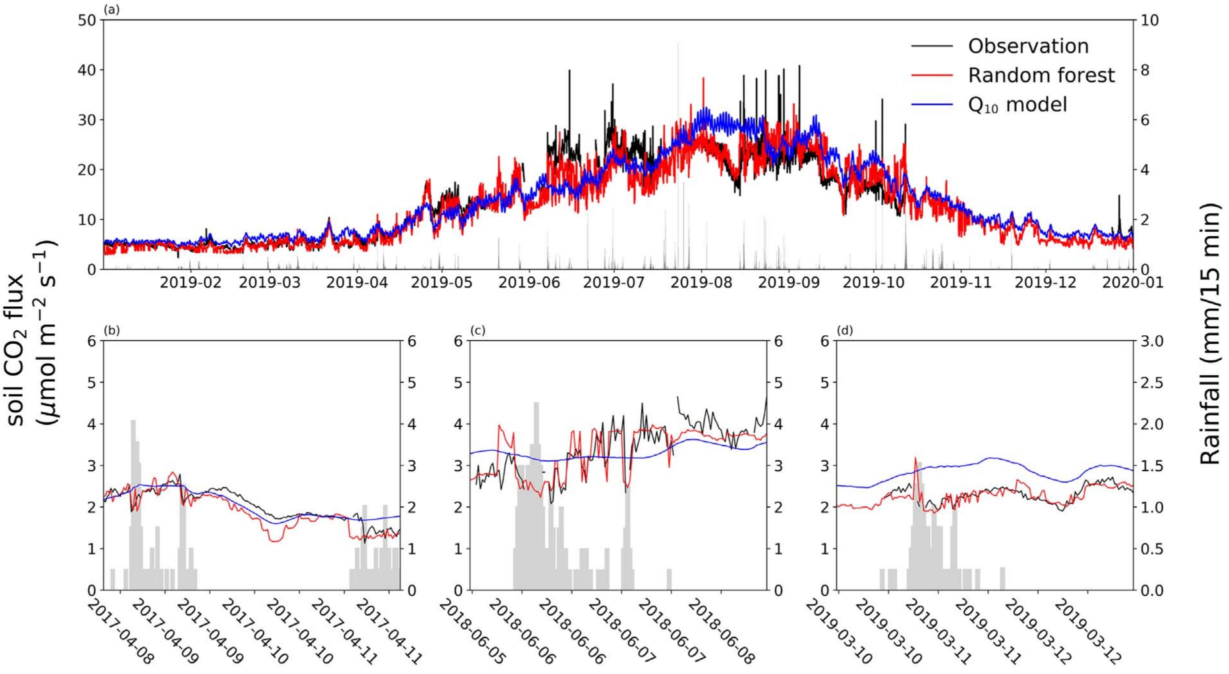

Figure 5. Time series of measured and predicted soil CO_2 fluxes. (a) Annual soil respiration times series in 2019. (b–d) Representative daily series of soil respiration containing chamber data blank.

model is 0.84 and 0.89 for the canopy-wet and canopy-dry periods, respectively; R^2 of Q_{10} model is 0.26 and 0.41 for the canopy-wet and canopy-dry period, respectively. Therefore, the RF gap-filled R_s dataset was used to replace the Q_{10} model-simulated R_s in the multilayer model. In this way, the influence of rainfall on R_s can be excluded in the simulated NEE, which will help improve the validity of comparing simulated and measured NEE to evaluate wet canopy photosynthesis. The average R_s of the three sampling plots after gap-filling by the RF model is 2.3, 2.8 and 2.7 μmol m^{-2} s^{-1} corresponding to the canopy-dry period, canopy-wet period during rainfall, and the canopy-wet period after rainfall, respectively.

Gas exchange in different interception situations

The multilayer model performed well in predicting the canopy-dry period NEE (Table 2 and Fig. 6a). The four models had the same output during canopy-dry period (overlapped dots in Fig. 6a). For the canopy-wet period, the NEE simulated with Model 2 had the closest average to the observed value. In addition, the MAE, RMSE, and the coefficient of determination (R^2) were linked to the greatest precision of Model 2 (Table 2). This forest had an increasing CO_2 uptake along with the enhancement of R_n in both canopy-dry and canopy-wet periods, while both R_n and NEE during rainfall varied in a smaller range than in other periods and showed positive values when R_n was small (Fig. 6b). Similar to the trends of MAE, RMSE and R^2 in Table 2, the simulated NEE of Model 2 was the most precise in relation to R_n at both the during-rainfall and post-rainfall canopy-wet periods (Fig. 6b–e). R^2 is estimated based on the difference between observed and simulated values as well as the difference between each observed point and the average of observed value in each group. The difference between observed and simulated values, which can also be reflected by RMSE, was only a bit smaller in dry time than in wet

Table 2. The average observed (EC) and simulated NEE of the four models (17 October 2016 to 31 December 2019), RMSE, MAE and the coefficient of determination (R^2) between the observed and simulated NEE of the four models in the canopy-dry and canopy-wet periods.

		Average value (μmol m^{-2} s^{-1})	MAE (μmol m^{-2} s^{-1})	RMSE (μmol m^{-2} s^{-1})	R^2
Dry	EC	−7.75			
	Model 1	−8.34	3.18	4.51	0.23
	Model 2	−8.32	3.19	4.52	0.23
	Model 3	−8.29	3.19	4.51	0.23
	Model 4	−8.25	3.20	4.52	0.23
Wet	EC	−3.33			
	Model 1	−5.87	4.10	5.79	−0.09
	Model 2	−3.00	3.02	4.73	0.28
	Model 3	−0.42	4.27	5.78	−0.08
	Model 4	0.48	4.55	6.02	−0.17

time for Model 2. The difference between each observed point and the average of observed value in each group can be reflected by variance. The variance of observed NEE in dry time is 26.6; while the variance of observed NEE in wet time is 30.8. Given the similar RMSE, the smaller R^2 of dry time is mainly dominated by the smaller difference between the sum of each observed point and the average of observed value in each group (the smaller variance). In the same way, the larger difference between observed and simulated NEE presented by RMSE of Model 1, Model 3 and Model 4 make them a smaller R^2 in wet time than dry time. Based on these results, it is not enough to evaluate the model precision only by comparing R^2. Therefore, as a more straightforward way of demonstrating the difference between simulated and observed data, we also compared the simulated and observed NEE in relationship with R_n, as shown in Fig. 6.

The simulated NEE was the closest to the measured NEE in Model 2 during and after different levels of rainfall (Fig. 7). The rainfall intensity that results in the wetness in the daytime (08:00 to 16:00 h) was 0.5 mm/12 h, 3.0 mm/12 h, 13.7 mm/12 h and 55.1 mm/12 h for Event 1, 2, 3 and 4, respectively. For Event 1, R^2 between the measured and simulated NEE is 0.39, 0.31, 0.10 and 0.11, for Model 1, 2, 3 and 4, respectively; for Event 2, R^2 between the measured and simulated NEE is −0.74, 0.22, 0.47 and 0.38, for Model 1, 2, 3, and 4, respectively; for Event 3, R^2 between the measured and simulated NEE is 0.54, 0.86, 0.81 and 0.79, for Model 1, 2, 3 and 4, respectively; for Event 4, R^2 between the measured and simulated NEE is 0.34, 0.81, 0.57 and 0.40, for Model 1, 2, 3 and 4, respectively. Corresponding to the model setting of maximum leaf water storage capacity and wettable area, the simulated abaxial wet leaf area fraction, which represents the percentage of wet area per unit leaf area, showed advent differences among the four models (Fig. 7). Model 1 showed little wet leaf area all the time. Models 2 and 3 have a similar wet time but distinctive wet leaf area fractions. Models 3 and 4 have similar abaxial wet leaf fractions during the wet, but Model 4 has a larger abaxial wet leaf fraction at the end of a wetting event and longer simulated wet time.

The models showed high coupling with the measured λE during rainfall (Fig. 8b). For the canopy-wet period after small rain (Fig. 8c), R^2 between the measured and simulated λE is 0.44, 0.39, 0.29 and 0.12, for Model 1, 2, 3 and 4, respectively; for the canopy-wet period after middle rain (Fig. 8d), R^2 between the measured and simulated λE is 0.55, 0.54, 0.45 and 0.54, for Model 1, 2, 3 and 4, respectively; for the canopy-wet period after heavy rain (Fig. 8e), R^2 between the measured and simulated λE is 0.45, 0.56, 0.56 and 0.59, for Model 1, 2, 3 and 4, respectively. For the wet canopy during rainfall, all four models exhibited similar MAE, RMSE and R^2 values. However, Model 1 had the largest R^2 after low and moderate rainfall, whereas Model 4 had the largest R^2 after heavy rainfall (Table 3).

Seasonal change of CO_2 flux

Figure 9 shows the seasonal changes in the monthly average NEE by observation and simulation. The observed NEE of the canopy-wet period after rainfall (Fig. 9c) has a similar seasonal change trend to that of the canopy-dry period (Fig. 9a), although the observed NEE of the canopy-dry period was larger than that of the canopy-wet period in all seasons. Averaged monthly NEE of the canopy-wet period during rainfall is seldom lower than −5 μmol m^{-2} s^{-1}, while averaged monthly NEE of the canopy-dry period during rainfall can be less than −10 μmol m^{-2} s^{-1}.

The NEE simulated with Model 2 was closest to the observed NEE throughout the seasons during the canopy-wet periods (Fig. 9b and c). The seasonal trend of Model 1, which represented all stomata free from water blockage during the canopy-wet period, showed an obvious overestimation of CO_2 uptake. In contrast, the seasonal trends of Models 3 and 4, in which interception can culminate in the entire abaxial surface, showed an apparent underestimation of CO_2 uptake. Model 3, which had a smaller leaf water storage capacity, performed better than Model 4 during the canopy-wet periods after rainfall.

Discussion

Uncertainties

The acquisition of measurements and modelling are processes that can be impacted by a wide range of uncertainties. This is especially true in the context of this study, since there is a lack of widely recognized, systematic, and standardized methods for observing and evaluating canopy wetness and wet-leaf photosynthesis. In the context of the modelling efforts outlined in this study, gas exchange parameters were obtained from dry leaves. This approach was applied to circumvent the difficulty that underlies acquiring photosynthesis-related measurements from wet leaves. Correspondingly, this model operates on the assumption that gas exchange only occurs from the

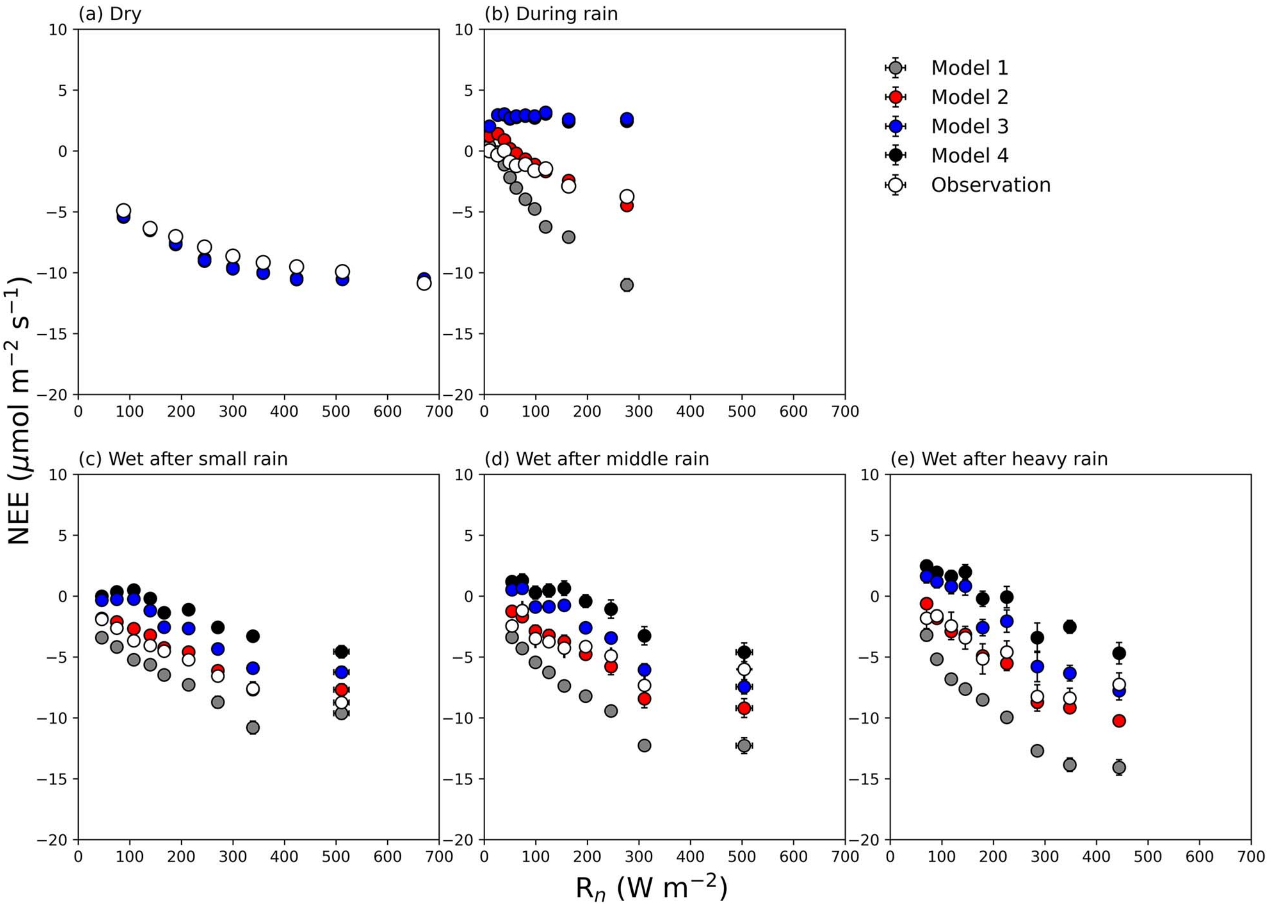

Figure 6. Relationship between net radiation (R_n) and NEE at different wet periods. (a) Canopy-dry; (b) canopy-wet during rainfall; (c) canopy-wet after small rainfall; (d) canopy-wet after middle rainfall; (e) canopy-wet after heavy rainfall. The dots represent the average of 30-min interval NEE. The error bar represents the standard error.

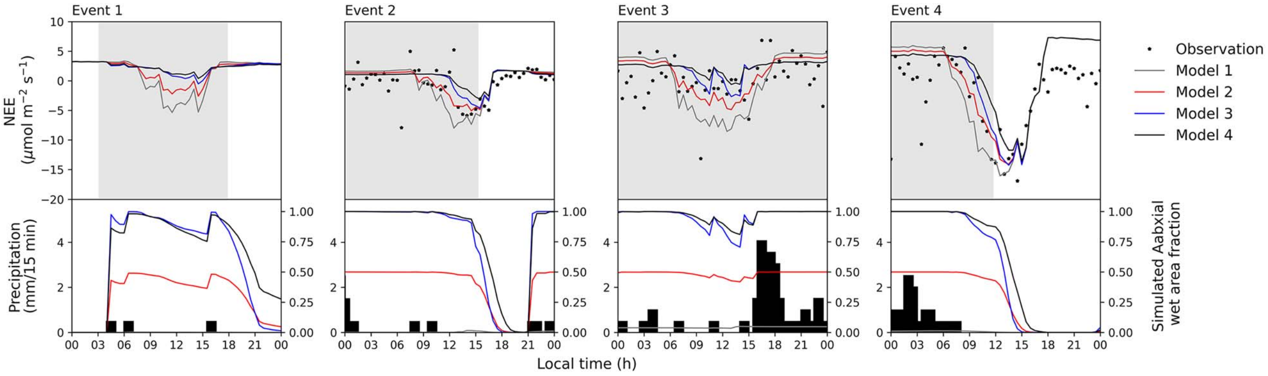

Figure 7. Daily series of measured and simulated NEE with the change of precipitation and simulated abaxial wet area fraction (which is estimated by Eq. A.65 in Appendix A.6; the maximum among top, middle, and bottom canopy layer was presented). The shadowed area indicates the canopy-wet period.

dry surfaces of the wet leaves; this is meant to guarantee the validity of the modelled gas exchange parameters and stomatal conductance (g_s). Based on the increased canopy conductance of the dry canopy immediately after wetness ended at the same site (Jiao et al. 2021), we tested NEE of the four models when the simulated g_s were increased by adjusting the value of m in Equation A.25 (a ball-type model) to ensure current g_s modelling is appropriate and the possible error in parameter value has little influence on our results. The increased g_s led to a larger overestimated CO_2 uptake in dry time NEE (Fig.A.9.1a and Fig. A.9.2a), but it did not bring much change to the differences among the four models in wet time. Model 2 still shows the closest value to the observed NEE even when the simulated g_s is largely raised among the four models. Model 1 has a larger overestimation of CO_2 uptake with the increased g_s compared with that in Fig. 6b and c, while Models 3 and 4 exhibit nonnegligible underestimated NEE like before improving g_s (Fig. 6b and c). This means the increased g_s (in reasonable range) will not change the difference of the four models caused by different abaxial interception. Thus, current g_s modelling is reasonable. In term of canopy evapotranspiration and interception, two parameters are considered

Table 3. Average of observed (EC) and simulated λE of the four models (i.e. from 17 October 2016 to 31 December 2019), including the RMSE, MAE and the coefficient of determination (R^2) between the observed and simulated NEE of the four models in canopy-dry and canopy-wet periods.

	Data	Average value ($\mathrm{W\ m^{-2}}$)	MAE ($\mathrm{W\ m^{-2}}$)	RMSE ($\mathrm{W\ m^{-2}}$)	R^2
Dry	EC	108.4 ± 0.7			
	Model 1	107.4 ± 0.7	17.3	23.1	0.90
	Model 2	108.13	17.53	23.7	0.86
	Model 3	107.21	17.34	23.26	0.86
	Model 4	108.1 ± 0.7	17.5	23.7	0.90
During rainfall	EC	72.1 ± 4.2			
	Model 1	69.0 ± 4.1	40.8	68.4	0.26
	Model 2	77.34	40.66	66.95	0.29
	Model 3	71.59	39.43	64.29	0.35
	Model 4	76.2 ± 4.1	40.4	66.4	0.30
After little rain	EC	127.3 ± 4.2			
	Model 1	119.1 ± 3.8	53.4	75.8	0.44
	Model 2	146.34	59.16	85.43	0.29
	Model 3	139.47	53.95	79.16	0.39
	Model 4	160.8 ± 5.3	62.0	95.0	0.12
After moderate rain	EC	105.0 ± 6.1			
	Model 1	85.1 ± 5.2	43.4	65.9	0.55
	Model 2	108.73	41.84	66.99	0.54
	Model 3	104.23	41.57	66.89	0.54
	Model 4	117.5 ± 7.0	42.7	72.6	0.45
After heavy rain	EC	127.7 ± 6.8			
	Model 1	93.2 ± 4.5	57.3	78.8	0.45
	Model 2	116.08	49.28	70.47	0.56
	Model 3	110.83	50.04	70.60	0.56
	Model 4	123.4 ± 5.4	47.6	68.2	0.59

responsible for the basic model. First, the bulk coefficient for sensible heat transfer (C_b) is a key parameter influencing the difference in water vapour flux among different adjacent canopy layers (Eqs A.10 and A.11). Thus, the value of C_b affects the evaporation rate in the model (recovering from canopy-wet to canopy-dry condition). Second, W_{Umax} is the maximum leaf water storage by the adaxial (upper) leaf surface. It is the key parameter deciding the leaf interception because the maximum leaf water storage by the abaxial surface is set as a certain ratio of the adaxial leaf surface in the four models (100% for Model 1, 2, 4, and 50% for Model 3). So W_{Umax} not only decides the basic amount for interception evaporation but also the time that leaf wetness blockage on stomata. The output value of the four models all changed a bit after decreasing or increasing the value of C_b and W_{Umax} (Tables A.9.2 and A.9.3). However, the differences among the four models remain the same as presented in Fig. 6.

Nevertheless, it should also be noted that the abaxial surface may actually has a smaller water storage capacity than the adaxial surface. This can explain the systematical difference between Model 2 and observed NEE that always exists after rainfall (Fig. 6c–e). Data of Model 2 in Fig. 6c–e are combined in Fig. 10. At the canopy-wet periods after rainfall, larger MAE (less precise prediction of NEE) was more likely to appear with high R_n and small abaxial wet area fraction, which often happened at the end of a wetting event. This error may be resulted by the same leaf water storage capacity (0.18 mm per unit leaf area) that was applied in both abaxial and adaxial surfaces in simulation. Thus, the lower leaf surfaces may already turn to be dry when near the end of the simulated wet period.

In addition to the potential uncertainty in modelling, the precise measurement of canopy wetness is challenging; in practice, this could culminate in a scenario in which some wet leaves are not detected by the sensors. On the one hand, the limited number of sensors is hard to precisely represent the whole canopy, especially for the leaves without sensor attached (Jiao et al. 2022). On the other hand, the sensors detect the presence of surface moisture on the sensor instead of directly detecting wet leaves. There are a host of differences between the sensors and leaves which cause possible differences in energy balance and surface-moisture interaction which lead to the possibility of sensor misrepresenting leaf wetness. In this case, a small difference may have arisen between the actual and simulated fluxes because of the time lag required to reach the actual drying point. To mitigate this risk, we strategically placed a substantial number of sensors at different heights in the canopy. Moreover, when we compared the simulation and observation, the absence of stomatal conductance measurements and abaxial wetness made it difficult to infer the mechanism underlying the observed reduction in photosynthesis.

Difference among CO_2 flux and λE from the wet Japanese cypress canopy

Two distinct differences are presented by λE simulation compared with NEE. First, simulated λE of different interception solutions all had a similar performance during rainfall (Fig. 8b), while simulated NEE of the four different models can be well distinguished from each other except Models 3 and 4 (Fig. 6b), both of which had all the stomata blocked during rainfall. The same low R_n during rainfall restricts the partitioning of available energy to λE (van Dijk et al. 2015) and leads to a similar λE regardless of the amount and distribution of interception (Jiao et al. 2022). The NEE by observation and different simulations were close to each other when R_n was extremely low ($<100\ \mathrm{Wm^{-2}}$), but CO_2 uptake

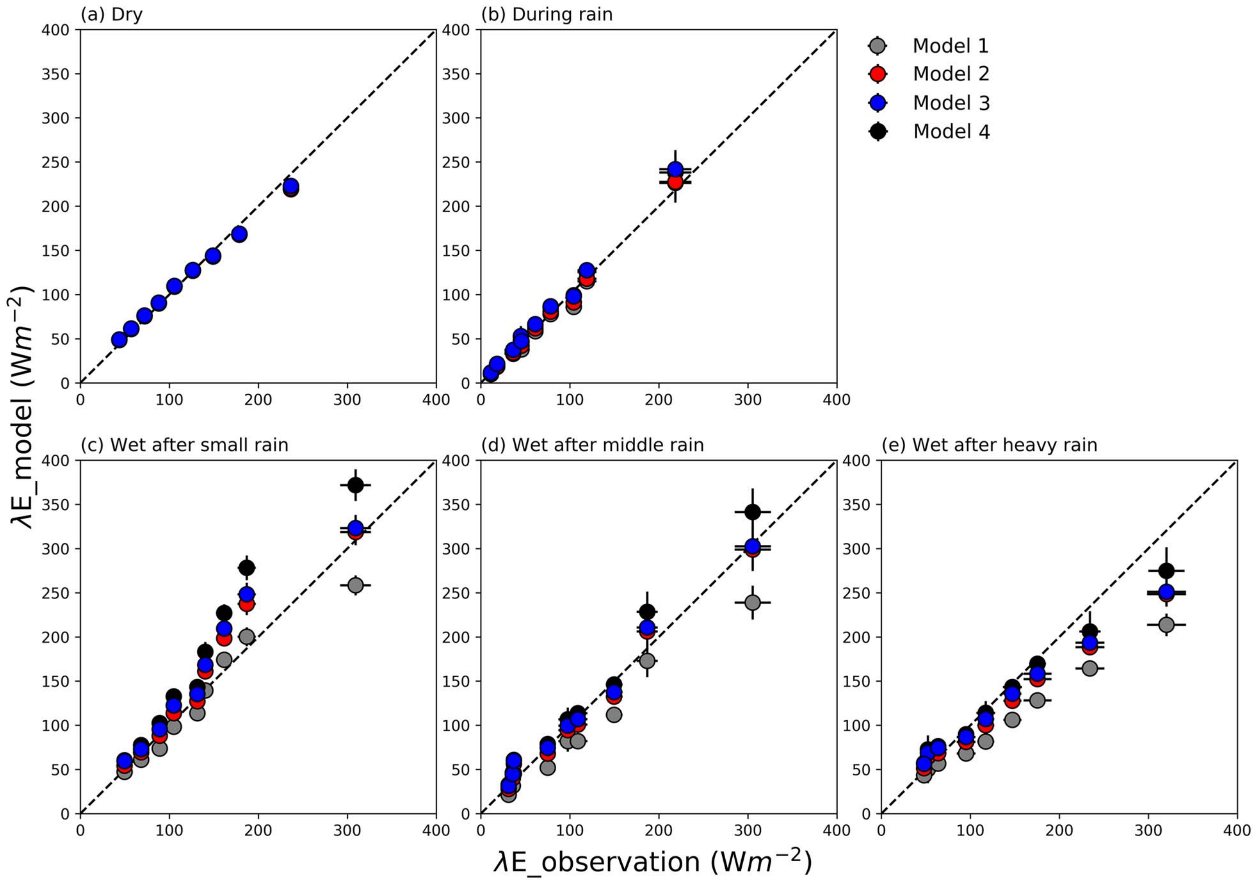

Figure 8. Regression between simulated and measured latent heat flux (λE) with different abaxial interception amount at different wet periods. (a) Canopy-dry; (b) canopy-wet during rainfall; (c) canopy wet after small rainfall; (d) canopy-wet after middle rainfall; (e) canopy-wet after heavy rainfall. The dots represent the average of 15-min interval λE. The error bar represents the standard error.

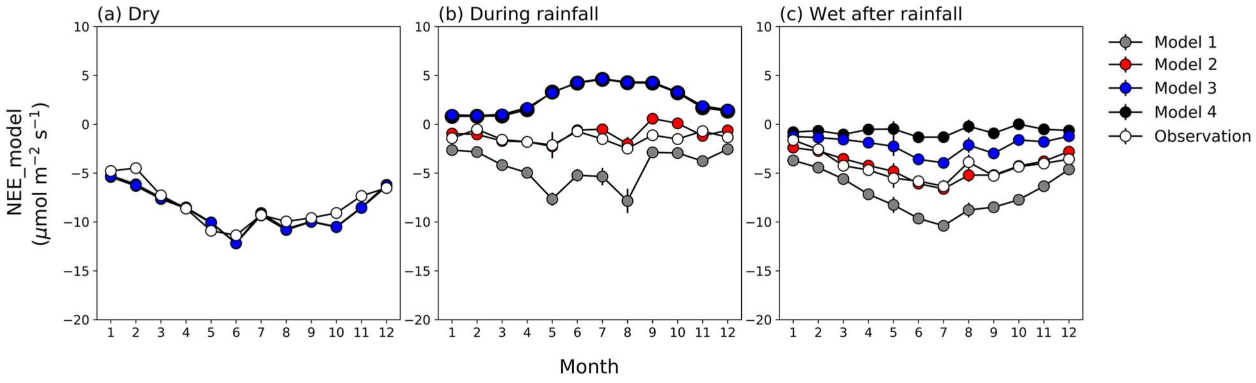

Figure 9. Average seasonal change of NEE determined by observation and simulation. The dots represent the average of 30-min interval NEE. The error bar represents the standard error.

still increased along with the improvement of R_n regardless of the period and rainfall intensity (Fig. 6). This means that even though some or all the abaxial stomatal pores of wet leaves are free from water blockage, the canopy can only maintain a reduced photosynthetic output when light and energy are inadequate.

Second, the simulated λE in the post-rainfall canopy-wet period with 100% of wet area on the abaxial leaf surface showed better precision after heavy rainfall than itself after small and middle rainfall (Model 4 in Fig. 8c–e), whereas Model 4 did not show such kind of trend in NEE simulation. Meanwhile, the simulated NEE always had the closest value to the observed NEE when the ratio of the wet area to the abaxial leaf was 50% (Model 2). Stronger rainfall intensity will also improve the amount of interception by branch and stem, which was not carefully considered in the model simulation but contained in the observed interception evaporation (wet canopy λE) and can be mistaken as leaf interception when comparing the simulation and observation. This might be the reason that Model 4 showed the best fitting for λE, whereas Model 2 showed the best fitting for NEE after heavy rain events. Hence, the simulation of λE could only verify the possible existence of abaxial leaf surface interception but could not precisely detect the corresponding interception amount or

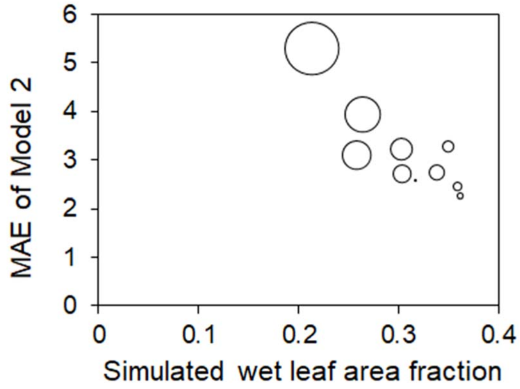

Figure 10. Relationship between the simulated abaxial wet area fraction and MAE of Model 2 in different range of net radiation (R_n). Data were extracted from Fig. 6c–e; each datapoint represents the average of 143 30-min interval data; the radius of each dot represents the average of R_n in each data group.

ratio. Combined with the NEE simulation, this study strongly suggests that a part of the abaxial leaf surfaces should be dry to explain CO_2 uptake during wet periods, even after heavy rainfall. The partially (i.e. 50%) wet leaf area on the abaxial surface seems valid, especially considering that rainfall is the main source of precipitation that occurs in this temperate forest. As a reference, even the leaf wetness measurement showed that the canopy of the Amazon rainforest (i.e. which is wet for longer, due to this region experiencing greater precipitation than that in the study site at hand) could not be completely wet most of the time (Binks et al. 2021). The coupling between NEE and λE also supports the validity of the gas exchange sub-model. Nevertheless, the further application of more precise leaf wetness measurements may allow for a more fine-scale elucidation of the dynamics that shape canopy wetness.

Reasons for wet Japanese cypress canopy maintaining photosynthesis

The CO_2 uptake from the wet canopy proved that the stomata were free of wetness and maintained gas exchange. This phenomenon can be explained in two ways. The first explanation is rooted in the consideration of the functional traits of the leaves. The 'xeromorphic' traits (hydrophobicity, stomatal crypts, stomatal clustering and the Florin rings around the stomatal pores), which could help the prevention of a water film forming over the stomata and prevent coverage of stomata by precipitation, is reported as a reason of *C. obtuse* maintaining photosynthesis in the cloud montane forest (Pariyar et al. 2017). Leaf traits have been shown to be closely related to leaf water storage capacity (Cavallaro et al. 2022), which has an impact on the simulation of wet canopy NEE, as shown by the sensitivity analysis (Appendix A.9). The superior performance of both λE and NEE from Model 3 compared with Model 4 after rainfall suggests that decreasing the abaxial water storage can also help improve the gas exchange model precision in certain range of maximum wet leaf area (Fig. 6c to d, 8c to d, 9c) because Models 3 and 4 both receive rainfall interception by the whole abaxial surface but Model 4 has a larger leaf water storage capacity. The smaller abaxial leaf water storage in Model 3 led to a shorter wet time than Model 4 (Fig. 7), which can be the reason that Model 3 NEE is closer to Model 2 and observation than Model 4. Future studies should also improve the parameters related to abaxial leaf water storage and evaluate how they will couple with the ratio of the wet area on the abaxial surface during a simulation (e.g. a combination between Models 2 and 3). In addition, the smaller abaxial leaf water storage capacity resulting from these traits can be beneficial for photosynthesis in the canopy-wet period after rainfall because a smaller leaf water storage capacity translates to smaller amount of interception and a shorter drying time of the abaxial surface.

Another reason, which is also the primary proposition brought forth in this study, is the lower rainfall interception on the abaxial side of the leaf than on its adaxial side. In contrast to the frequently occurring fog in cloud montane forests, which can form a water film over the entire abaxial and adaxial leaf surfaces, rainfall interception in temperate forests most directly occur on the adaxial leaf surface rather than on both leaf surfaces. Therefore, whether rainfall interception can be distributed on the abaxial surface should be considered prior to the clustering of hydrophobicity and leaf function traits in forests, where rainfall is the dominant precipitation. The CO_2 uptake of the wet canopy was overestimated when there was no abaxial interception (Model 1), whereas the CO_2 uptake of the wet canopy was underestimated when interception occurred on the entire abaxial surface (Models 3 and 4). The best performance of Model 2 in predicting the observed NEE among the four models suggests that only half of the per-leaf area in the Japanese cypress canopy can be wetted by interception. Thus, some of the stomata on the dry surface can keep a certain aperture to help the wet canopy maintain photosynthesis, which is also a reason for the depressed photosynthesis during the canopy-wet period compared with the canopy-dry period.

Through other leaf-level experiments, different leaf functional traits of the abaxial and adaxial surfaces were also found to be related to wet leaf photosynthesis and leaf wettability in other species besides the Japanese cypress (Holder 2012; Aparecido et al. 2017). The contribution of these traits to variations in wet canopy gas exchange across different regions, in the context of global climate change, has rarely been discussed; however, these processes are worthy of further investigation. Although some studies have focused on how leaf traits of different species influence leaf water storage capacity and leaf wetness duration (Rosado and Holder 2013; Holder 2012; Smith and McClean 1989), few have reported interception (i.e. as facilitated by the abaxial leaf surface) of different species. The distribution of the wet area on the abaxial leaf surface of other conifers (e.g. needles, rather than scales) may differ from that of Japanese cypress. The results of this study suggest that the relationship between abaxial leaf wetness and leaf morphology should also be considered when investigating wet canopy (leaf) gas exchange in areas where rainfall is the dominant form of precipitation.

Effect of rainfall-induced leaf wetness on canopy photosynthesis

The increased photosynthesis, presented by higher canopy conductance (g_c) and smaller negative NEE, was also reported in the first 3 h immediately after canopy wetness ended in the dry canopy of the same Japanese cypress forest (Jiao et al. 2021). The increased g_c immediately after the end of wetting suggests a larger stomatal conductance than the usual dry period, which can be explained by decreased vapour pressure deficit and foliar water uptake (Kawamitsu et al. 1993; Munne-Bosch et al. 1999; Hanba et al. 2004; Breshears et al. 2008; Berry et al. 2014; Chu et al. 2014; Gerlein-Safdi et al. 2018). In contrast, the excellent performance of Model 2 (i.e. in the simulation of NEE) suggests that interception-induced leaf wetness reduced the photosynthetic activity of the Japanese cypress forest canopy; this reduction could have occurred because some of the stomates were covered with water, resulted from rainfall interception. However, because of the limitations inherent in the measurement of stomatal conductance in humid environments (Aparecido et al. 2017), this study only proved that some of the stomates were blocked during and after rainfall, thus leading to depressed canopy photosynthesis rather than directly presenting a decreased stomatal conductance change during and after rainfall. With the uncertainties of g_s modelling in this study, future studies should also consider how the actual stomatal conductance of these water-free abaxial leaf areas changes during and after rainfall as well as improving the g_s simulation and observation of the partly wetted leaves.

The depressing effect of interception-induced leaf wetness on wet canopy photosynthesis did not change the seasonal regulation of NEE, and the wet canopy after rainfall still had a smaller NEE in spring and summer than in autumn and winter (Fig. 9). The average observed NEE in Fig. 9 also indicates that the wet canopy CO_2 uptake is mainly due to photosynthesis during the post-rainfall canopy-wet period, rather than during the rainfall period. According to this seasonal average, the accumulated daytime CO_2 uptake based on the average daytime NEE of the canopy-dry period, canopy-wet period during rain, and canopy-wet period after rainfall throughout the year were calculated as −2255, −36 and −298 gC m^{-2} $year^{-1}$, respectively. The canopy-wet period during rainfall and the canopy-wet period after rainfall contributed 1% and 11% of the average annual NEE and 7% and 17% of the total time, respectively. Also, considering the similar average soil CO_2 emission at the canopy-wet period after rainfall (2.8 μmol m^{-2} s^{-1}) and canopy-wet period during rainfall (2.7 μmol m^{-2} s^{-1}), the canopy photosynthesis after rainfall period had the dominant contribution to wet canopy CO_2 uptake. On one hand, the canopy-wet period after rainfall represented more of the total canopy-wet time than the during-rainfall period, which should have contributed to CO_2 uptake. However, under the condition that stomata can maintain their opening during and after rainfall, photosynthetic activities will benefit from the recovery of meteorological conditions when rainfall ends (e.g. a larger range of R_n in Fig. 6). Moreover, although the 30-min time series of NEE sometimes did not show clear CO_2 uptake during canopy-wet periods (e.g. Event 1 in Fig. 7), notable CO_2 uptake (−334 gC m^{-2} $year^{-1}$) was found after accumulating daytime NEE of canopy-wet periods in a year. Therefore, the contribution of wet canopy CO_2 uptake should be considered when estimating long-term forest carbon exchange along with the changing climate.

Conclusions

Using the EC method with an enclosed-path gas analyser, we found that photosynthesis was reduced during the canopy-wet period. The simulation of NEE with different abaxial wet area ratios and leaf water storage capacities based on an SVAT multilayer model showed that 50% of the per abaxial leaf area in the Japanese cypress canopy could be wetted during and after rainfall. However, this wetting could only occur under the condition that the abaxial and adaxial surfaces had the same leaf water storage capacity. This finding shows that that rainfall interception can form a water film over part of the stomata on the leaves of Japanese cypress. A notable accumulation in CO_2 uptake was observed during the wet period. In addition, a larger CO_2 uptake was observed in the post-rainfall canopy-wet period than in the during-rainfall period. This indicates that photosynthesis in the wet canopy occurred more readily after rainfall than during rainfall. Different from the 'xeromorphic' traits that may help Japanese cypress keep stomatal free from fog or condensation-induced leaf wetness, this study showed the distribution and amount of interception on the abaxial surface is an important factor that influences the wet canopy photosynthesis relating to rainfall. However, stomatal conductance and photosynthesis-related physiological changes underlying the functioning of these partly wetted leaves are still not well understood and are worthy of further investigation. Overall, these findings are expected to contribute towards the improvement of ecosystem carbon exchange models, particularly in terms of the effect of rainfall on forest carbon circulation in the context of a changing climate.

Acknowledgments

We sincerely thank Dr. Katsunori Tanaka for his comments on improving the multilayer model. We sincerely thank Prof. Kanehiro Kitayama and Prof. Kaoru Kitajima of Kyoto University for their comments on improving this manuscript. We appreciate the anonymous reviewers for their constructive comments on improving this manuscript.

Funding

This work was supported by a Japan Society for the Promotion of Science (JSPS) Grant-in-Aid for Scientific Research (KAKENHI:20H00434), the Coca-Cola Foundation, and the project 'Development of technology for impacts, mitigation and adaptation to climate change in the sectors of agriculture, forestry and fisheries'of Agriculture, Forestry and Fisheries Research Council partially. L.J. was supported by the China Scholarship Council (No.20200805018).

Conflict of interest

None declared.

Data availability

The data that support the findings of this study are available from the corresponding author upon reasonable request.

References

Amiro BD, Barr AG, Black TA, Iwashita H, Kljun N, McCaughey JH, Morgenstern K, Murayama S, Nesic Z, Orchansky AL, et al. 2006. Carbon, energy and water fluxes at mature and disturbed forest sites, Saskatchewan, Canada. Agric For Meteorol. 136(3–4): 237–251. https://doi.org/10.1016/j.agrformet.2004.11.012.

Aparecido LMT, Miller GR, Cahill AT, Moore GW. 2017. Leaf surface traits and water storage retention affect photosynthetic responses to leaf surface wetness among wet tropical forest and semiarid savanna plants. Tree Physiol. 37(10):1285–1300. https://doi.org/10.1093/treephys/tpx092.

Aubinet M. 2008. Eddy covariance CO_2 flux measurements in nocturnal conditions: an analysis of the problem. Ecol Appl. 18(6): 1368–1378. https://doi.org/10.1890/06-1336.1.

Baldocchi DD, Hutchison BA. 1986. On estimating canopy photosynthesis and stomatal conductance in a deciduous forest with clumped foliage. Tree Physiol. 2(1–2–3):155–168. https://doi.org/10.1093/treephys/2.1-2-3.155.

Baldocchi DD, Xu L. 2007. What limits evaporation from Mediterranean oak woodlands – the supply of moisture in the soil, physiological control by plants or the demand by the atmosphere? Adv Water Resour. 30(10):2113–2122. https://doi.org/10.1016/j.advwatres.2006.06.013.

Baldocchi D, Falge E, Gu L, Olson R, Hollinger D, Running S, Anthoni P, Bernhofer C, Davis K, Evans R, Fuentes J, et al. 2001. FLUXNET: a new tool to study the temporal and spatial variability of ecosystem-scale carbon dioxide, water vapor, and energy flux densities. Bull Am Meteorol Soc. 82(11):2415–2434. https://doi.org/10.1175/1520-0477(2001)082<2415:FANTTS>2.3.CO;2.

Ball, J.T., Woodrow, I.E., Berry, J.A., 1987. A model predicting stomatal conductance and its contribution to the control of photosynthesis under different environmental conditions. In Progress in photosynthesis research. J. Biggins. Ed. Dordrecht: Springer, pp. 221–224. https://doi.org/10.1007/978-94-017-0519-6_48

Berry ZC, Goldsmith GR. 2020. Diffuse light and wetting differentially affect tropical tree leaf photosynthesis. New Phytol. 225(1): 143–153. https://doi.org/10.1111/nph.16121.

Berry ZC, White JC, Smith WK. 2014. Foliar uptake, carbon fluxes and water status are affected by the timing of daily fog in saplings from a threatened cloud forest. Tree Physiol. 34(5):459–470. https://doi.org/10.1093/treephys/tpu032.

Binks O, Finnigan J, Coughlin I, Disney M, Calders K, Burt A, Vicari MB, da Costa AL, Mencuccini M, Meir P. 2021. Canopy wetness in the eastern Amazon. Agric For Meteorol 297:108250. https://doi.org/10.1016/j.agrformet.2020.108250.

Breiman L. 2001. Random forests. Mach Learn 45(1):5–32. https://doi.org/10.1023/A:1010933404324.

Breshears DD, McDowell NG, Goddard KL, Dayem KE, Martens SN, Meyer CW, Brown KM. 2008. Foliar absorption of interrcepted rainfall improves woody plant water status most during drought. Ecology. 89(1):41–47. https://doi.org/10.1890/07-0437.1.

Brooks A, Farquhar GD. 1985. Effect of temperature on the CO_2/O_2 specificity of ribulose-1,5-bisphosphate carboxylase/oxygenase and the rate of respiration in the light - estimates from gas-exchange measurements on spinach. Planta. 165(3):397–406. https://doi.org/10.1007/BF00392238.

Burba, G. 2013. Eddy covariance method for scientific, industrial, agricultural, and regulatory applications: a field book on measuring ecosystem gas exchange and areal emission rates. LI-COR Biosciences, Lincoln, Nebraska.

Burba GG, Medermitt DK, Anderson DJ, Furtaw MD, Eckles RD. 2010. Novel design of an enclosed CO_2/H_2O gas analyser for eddy covariance flux measurements. Tellus B, 62(5):743–748. https://doi.org/10.1111/j.1600-0889.2010.00468.x.

Cavallaro A, Carbonell-Silletta L, Burek A, Goldstein G, Scholz FG, Bucci SJ. 2022. Leaf surface traits contributing to wettability, water interception and uptake of above-ground water sources in shrubs of Patagonian arid ecosystems. Ann Bot. 130(3):409–418. https://doi.org/10.1093/aob/mcac042.

Chu H-S, Chang S-C, Klemm O, Lai C-W, Lin Y-Z, Wu C-C, Lin J-Y, Jiang J-Y, Chen J, Gottgens JF, et al. 2014. Does canopy wetness matter? Evapotranspiration from a subtropical montane cloud forest in Taiwan. Hydrol Process. 28(3):1190–1214. https://doi.org/10.1002/hyp.9662.

Curiel Yuste J, Janssens IA, Carrara A, Ceulemans R. 2004. Annual Q10 of soil respiration reflects plant phenological patterns as well as temperature sensitivity. Glob Chang Biol. 10(2):161–169. https://doi.org/10.1111/j.1529-8817.2003.00727.x.

Davidson EA, Janssens IA, Lou Y. 2006. On the variability of respiration in terrestrial ecosystems: moving beyond Q10. Glob Chang Biol. 12(2):154–164. https://doi.org/10.1111/j.1365-2486.2005.01065.x.

Dawson TE, Goldsmith GR. 2018. The value of wet leaves. New Phytol. 219(4):1156–1169. https://doi.org/10.1111/nph.15307.

Dreyer E, Le Roux X, Montpied P, Daudet FA,. Masson F, 2001. Temperature response of leaf photosynthetic capacity in seedlings from seven temperate tree species. Tree Physiol 214:223–232. https://doi.org/10.1093/treephys/21.4.223, .

Fang C, Moncrieff JB. 2001. The dependence of soil CO_2 efflux on temperature. Soil Biol Biochem. 33(2):155–165. https://doi.org/10.1016/S0038-0717(00)00125-5.

Farquhar GD, Wong SC. 1984. An empirical model of stomatal conductance. Funct Plant Biol. 11(3):191–210. https://doi.org/10.1071/PP9840191.

Farquhar GD, von Caemmerer S, Berry JA. 1980. A biochemical model of photosynthetic CO_2 assimilation in leaves of C3 species. Planta. 149(1):78–90. https://doi.org/10.1007/BF00386231.

Fei X, Song Q, Zhang Y, Liu Y, Sha L, Yu G, Zhang L, Duan C, Deng Y, Wu C, et al. 2018. Carbon exchanges and their responses to temperature and precipitation in forest ecosystems in Yunnan, Southwest China. Sci Total Environ. 616–617:824–840. https://doi.org/10.1016/j.scitotenv.2017.10.239.

Foken T, Wichura B. 1996. Tools for quality assessment of surface-based flux measurements. Agric For Meteorol. 78(1–2):83–105. https://doi.org/10.1016/0168-1923(95)02248-1.

Gerlein-Safdi C, Koohafkan MC, Chung M, Rockwell FE, Thompson S, Caylor KK. 2018. Dew deposition suppresses transpiration and carbon uptake in leaves. Agric For Meteorol. 259:305–316. https://doi.org/10.1016/j.agrformet.2018.05.015.

Hanba YT, Moriya A, Kimura K. 2004. Effect of leaf surface wetness and wettability on photosynthesis in bean and pea. Plant Cell Environ. 27(4):413–421. https://doi.org/10.1046/j.1365-3040.2004.01154.x.

Harley PC, Baldocchi DD. 1995. Scaling carbon dioxide and water vapour exchange from leaf to canopy in a deciduous forest. I. Leaf model parametrization. Plant Cell Environ. 18(10):1146–1156. https://doi.org/10.1111/j.1365-3040.1995.tb00625.x.

Harley PC, Thomas RB, Reyanolds JF, Strain BR. 1992. Modelling photosynthesis of cotton grown in elevated CO_2. Plant Cell Environ. 15(3):271–282. https://doi.org/10.1111/j.1365-3040.1992.tb00974.x.

Holder CD. 2012. The relationship between leaf hydrophobicity, water droplet retention, and leaf angle of common species in a semi-arid region of the western United States. Agric For Meteorol. 152:11–16. https://doi.org/10.1016/j.agrformet.2011.08.005.

Ishibashi M, Terashima I. 1995. Effects of continuous leaf wetness on photosynthesis: adverse aspects of rainfall. Plant Cell Environ. 18(4): 431–438. https://doi.org/10.1111/j.1365-3040.1995.tb00377.x.

Jarman PD. 1974. The diffusion of carbon dioxide and water vapour through stomata. J Exp Bot. 25(5):927–936. https://doi.org/10.1093/jxb/25.5.927.

Jiao L, Kosugi Y, Sempuku Y, Chang TW. 2021. Canopy conductance and gas exchange of a Japanese cypress forest after rainfall-induced wetness. Ecol Res. 36(6):947–960. https://doi.org/10.1111/1440-1703.12257.

Jiao L, Kosugi Y, Sempuku Y, Chang T, Chen S. 2022. Does interception evaporation occur from both sides of leaves at the wet Japanese cypress canopy during and after rainfall? Ecohydrology. 16(2). https://doi.org/10.1002/eco.2495.

Jordan DB, Ogren WL. 1984. The CO_2 /O_2 specificity of ribulose 1,5-bisphosphate carboxylase/oxygenase - dependence on ribulose-bisphosphate concentration, pH and temperature. Planta. 161(4): 308–313. https://doi.org/10.1007/BF00398720.

Katsuyama M, Ohte N, Kosugi Y, Tani M. 2021. The Kiryu experimental watershed: 50-years of rainfall-runoff data for a forest catchment in central Japan. Hydrol Process. 35(3). https://doi.org/10.1002/hyp.14104.

Kawamitsu Y, Yoda S, Agata W. 1993. Humidity pretreatment affects the responses of stomata and CO2 assimilation to vapor pressure difference in C3 and C4 plants. Plant Cell Physiol. 34:113–119. https://doi.org/10.1093/oxfordjournals.pcp.a078384.

Kim KW. 2018. Electron microscopic observations of stomata, epicuticular waxes, and papillae in *Chamaecyparis obtusa*: reconsidering the traditional concept of Y-shaped white stomatal bands. Microsc Res Tech. 81(7):716–723. https://doi.org/10.1002/jemt.23027.

Kimura K, Tanakamaru S. 1981. Studies on plant response to rainfall (II) effect of mist treatment on dry matter production on sunny days. J Agric Meteorol. 37(3):231–237. https://doi.org/10.2480/agrmet.37.231.

Komatsu H, Shinohara Y, Kume T, Otsuki K. 2008. Relationship between annual rainfall and interception ratio for forests across Japan. For Ecol Manage. 256(5):1189–1197. https://doi.org/10.1016/j.foreco.2008.06.036.

Kosugi Y, Matsuo N. 2006. Seasonal fluctuations and temperature dependence of leaf gas exchange parameters of co-occurring evergreen and deciduous. Tree Physiol. 26(9):1173–1184. https://doi.org/10.1093/treephys/26.9.1173.

Kosugi Y, Takanashi S, Matsuo N, Tanaka K, Tanaka H. 2006. Impact of leaf physiology on gas exchange in a Japanese evergreen broadleaved forest. Agric For Meteorol. 139(3–4):182–199. https://doi.org/10.1016/j.agrformet.2006.06.009.

Kosugi Y, Takanashi S, Tanaka H, Ohkubo S, Tani M, Yano M, Katayama T. 2007. Evapotranspiration over a Japanese cypress forest. I. Eddy covariance fluxes and surface conductance characteristics for 3 years. J Hydrol. 337(3–4):269–283. https://doi.org/10.1016/j.jhydrol.2007.01.039.

Kosugi Y, Takanashi S, Ueyama M, Ohkubo S, Tanaka H, Matsumoto K, Yoshifuji N, Ataka M, Sakabe A. 2013. Determination of the gas exchange phenology in an evergreen coniferous forest from 7 years of eddy covariance flux data using an extended big-leaf analysis. Ecol Res. 28(3):373–385. https://doi.org/10.1007/s11284-012-1019-4.

Lee MS, Nakane K, Nakatsubo T, Mo WH, Koizumi H. 2002. Effects of rainfall events on soil CO_2 flux in a cool temperate deciduous broad-leaved forest. Ecol Res. 17(3):401–409. https://doi.org/10.1046/j.1440-1703.2002.00498.x.

Leuning R. 1995. A critical appraisal of a combined stomatal - photosynthesis model for C3 plants. Plant Cell Environ. 18(4):339–355. https://doi.org/10.1111/j.1365-3040.1995.tb00370.x.

Lohammar T, Larsson S, Linder S, Falk SO. 1980. FAST: simulation models of gaseous exchange in scots pine. Ecol Bull. 32:505–523. http://www.jstor.org/stable/20112831.

Magarey RD, Russo JM, Seem RC, Gadoury DM. 2005. Surface wetness duration under controlled environmental conditions. Agric For Meteorol. 128(1–2):111–122. https://doi.org/10.1016/j.agrformet.2004.07.017.

Makita N, Kosugi Y, Sakabe A, Kanazawa A, Ohkubo S, Tani M. 2018. Seasonal and diurnal patterns of soil respiration in an evergreen coniferous forest: evidence from six years of observation with automatic chambers. PloS One. 13(2): e0192622. https://doi.org/10.1371/journal.pone.0192622.

McMillen RT. 1988. An eddy correlation technique with extended applicability to non-simple terrain. Boundary Layer Meteorol. 43(3):231–245. https://doi.org/10.1007/BF00128405.

Mellor GL, Yamada T. 1974. A hierarchy of turbulence closure models for planetary boundary layers. J Atmos Sci. 31(7):1791–1806. https://doi.org/10.1175/1520-0469(1974)031<1791:AHOTCM>2.0.CO;2.

Munne-Bosch S, Nogues S, Alegre L. 1999. Diurnal variations of photosynthesis and dew absorption by leaves in two evergreen shrubs growing in Mediterranean field conditions. New Phytol. 144(1):109–119. https://doi.org/10.1046/j.1469-8137.1999.00490.x.

Nakai T, Iwata H, Harazono Y. 2011. Importance of mixing ratio for a long-term CO_2 flux measurement with a closed-path system. Tellus B Chem Phys Meteorol. 63(3):302–308. https://doi.org/10.1111/j.1600-0889.2011.00538.x.

Nobel PS. 1991. Physicochemical and environmental plant physiology. San Diego, CA: Academic Press.

Pariyar S, Chang SC, Zinsmeister D, Zhou H, Grantz DA, Hunsche M, Burkhardt J. 2017. Xeromorphic traits help to maintain photosynthesis in the perhumid climate of a Taiwanese cloud forest. Oecologia. 184(3):609–621. https://doi.org/10.1007/s00442-017-3894-4.

Park J, Shin J-Y, Kim KR, Ha J-C. 2019. Leaf wetness duration models using advanced machine learning algorithms: application to farms in Gyeonggi Province, South Korea. Water. 11(9):1878. https://doi.org/10.3390/w11091878.

Rosado BHP, Holder CD. 2013. The significance of leaf water repellency in ecohydrological research: a review. Ecohydrology. 6(1): 150–161. https://doi.org/10.1002/eco.1340.

Ross J. 1975. Radiative transfer in plant communities. In: Monteith JL. Ed. Vegetation and atmosphere, Vol. 1, Academic Press, California, pp 13–55.

Saigusa N, Yamamoto S, Ryuichi H, Ohtani Y, Ide R, Asanuma J, Gamo M, Hirano T, Kondo H, Kosugi Y, et al. 2008. Temporal and spatial variations in the seasonal patterns of CO_2 flux in boreal , temperate , and tropical forests in East Asia. Agric For Meteorol. 148(5):700–713. https://doi.org/10.1016/j.agrformet.2007.12.006.

Sakabe A, Kosugi Y, Takahashi K, Itoh M, Kanazawa A, Makita N, Ataka M. 2015. One year of continuous measurements of soil CH_4 and CO_2 fluxes in a Japanese cypress forest: temporal and spatial variations associated with Asian monsoon rainfall. J Geophys Res Biogeogr. 120(4): 585–599. https://doi.org/10.1002/2014JG002851.

Sempuku Y, Kosugi Y, Iwata H, Tsuruta K, Kamakura M, Sakabe A. 2018. Evaluation of canopy evapotranspiration and photosynthesis during and immediately after rainfall using enclosed-path Eddy covariance method. J Japan Soc Hydrol Water Resour. 31(3):190–199 (in Japanese with English abstract). https://doi.org/10.3178/jjshwr.31.190.

Sharpe PJ, De Michele DW. 1977. Reaction kinetics of poikilotherm development. J Theor Biol. 64(4):649–670. https://doi.org/10.1016/0022-5193(77)90265-x.

Smith WK, McClean TM. 1989. Adaptive relationship between leaf water repellency, stomatal distribution, and gas exchange. Am J Bot. 76(3):465–469. https://doi.org/10.1002/j.1537-2197.1989.tb11335.x.

Song QH, Tan ZH, Zhang YP, Cao M, Sha LQ, Tang Y, Liang NS, Schaefer D, Zhao JF, Zhao JB, et al. 2013. Spatial heterogeneity of soil respiration in a seasonal rainforest with complex terrain. IForest. 6:65–72. https://doi.org/10.3832/ifor0681-006.

Takanashi S, Kosugi Y, Tani M, Ohte N, Yano M, Tanaka H, Tanaka K. 2003. Evapotranspiration from a Japanese cypress forest during and after rainfall. J Japan Soc Hydrol Water Resour. 16(3):268–283 (in Japanese with English abstract). https://doi.org/10.3178/jjshwr.16.268.

Takanashi S, Kosugi Y, Tanaka Y, Yano M, Katayama T, Tanaka H, Tani M. 2005. CO_2 exchange in a temperate Japanese cypress forest compared with that in a cool-temperate deciduous broadleaved forest. Ecol Res. 20(3):313–324. https://doi.org/10.1007/s11284-005-0047-8.

Tanaka K. 2002. Multi-layer model of CO_2 exchange in a plant community coupled with the water budget of leaf surfaces. Ecol Model. 147(1):85–104. https://doi.org/10.1016/S0304-3800(01)00413-6.

Tsuruta K, Kosugi Y, Takanashi S, Tani M. 2016. Inter-annual variations and factors controlling evapotranspiration in a temperate Japanese cypress forest. Hydrol Process. 30(26):5012–5026. https://doi.org/10.1002/hyp.10977.

Ueyama M, Kai A, Ichii K, Hamotani K, Kosugi Y, Monji N. 2011. The sensitivity of carbon sequestration to harvesting and climate conditions in a temperate cypress forest: observations and modeling. Ecol Model. 222(17):3216–3225. https://doi.org/10.1016/j.ecolmodel.2011.05.006.

Ueyama M, Hirata R, Mano M, Hamotani K, Harazono Y, Hirano T, Miyata A, Takagi K, Takahashi Y. 2012. Influences of various calculation options on heat, water and carbon fluxes determined by open- and closed-path eddy covariance methods. Tellus B. 64(1):19048. https://doi.org/10.3402/tellusb.v64i0.19048.

van Boxel JH, Sterk G, Arens SM. 2004. Sonic anemometers in aeolian sediment transport research. Geomorphology. 59(1–4):131–147. https://doi.org/10.1016/j.geomorph.2003.09.011.

van Dijk AIJM, Gash JH, van Gorsel E, Blanken PD, Cescatti A, Emmel, C, Gielen B, Harman IN, Kiely G, Merbold L, et al. 2015. Rainfall interception and the coupled surface water and energy balance. Agric For Meteorol 214–215:402–415. https://doi.org/10.1016/j.agrformet.2015.09.006.

von Caemmerer S, Farquhar GD. 1981. Some relationships between the biochemistry of photosynthesis and the gas exchange of leaves. Planta. 153(4):376–387. https://doi.org/10.1007/BF00384257.

Watanabe T. 1993. The bulk transfer coefficients over a vegetated surface based on k-theory and a 2nd-order closure model. J Meteorol Soc Japan. 71:33–42. https://doi.org/10.2151/jmsj1965.71.1_33.

Watanabe T, Kondo J. 1990. The influence of canopy structure and density upon the mixing length within and above vegetation. J Meteorol Soc Japan. 68(2):227–235. https://doi.org/10.2151/jmsj1965.68.2_227.

Watanabe T, Mizutani K. 1996. Model study on micrometeorological aspects of rainfall interception over an evergreen broad-leaved forest. *Agric For Meteorol*, 80(2–4), 195–214. https://doi.org/10.1016/0168-1923(95)02301-1.

Webb E, Leuning R. 1980. Correction of flux measurements for density effects due to heat and water vapour transfer. Q J Meteorol Soc. 106(447):85–100. https://doi.org/10.1002/qj.49710644707.

Wilczak JM, Oncley SP, Stage SA. 2001. Sonic anemometer tilt correction algorithms. Boundary Layer Meteorol. 99(1):127–150. https://doi.org/10.1023/A:1018966204465.

Wilson NR, Shaw RH. 1977. A higher order closure model for canopy flow. J Appl Meteorol. 16(11):1197–1205. https://doi.org/10.1175/1520-0450(1977)016<1197:AHOCMF>2.0.CO;2.

Wullschleger SD. 1993. Biochemical limitations to carbon assimilation in C3 plants—a retrospective analysis of the A/C$_i$ curves from 109 species. J Exp Bot. 44(5):907–920. https://doi.org/10.1093/jxb/44.5.907.

Zhang R, Huang J, Wang X, Zhang JA, Huang F. 2016. Effects of precipitation on sonic anemometer measurements of turbulent fluxes in the atmospheric surface layer. J Ocean Univ China. 15(3): 389–398. https://doi.org/10.1007/s11802-016-2804-4.

Appendices

Calculations underlying the seven sub-models of the original multilayer model (Model 1) by Tanaka (2002) and Kosugi et al. (2006) are described in Appendix A.1–A.7. Appendix A.8 brings forth the symbols, units, and values of the parameters used in the multilayer model in the simulation of canopy photosynthesis and soil respiration. Appendix A.9 presents the results of the sensitivity test conducted on three key parameters related to rainfall interception and leaf photosynthesis.

Sub-model (1): Reynolds stress, sensible heat exchange, leaf CO$_2$ and H$_2$O exchange and ground surface

By employing time and horizontal averages, the differences between adjacent homogeneous canopy planes (height $z, z + dz$) in the Reynolds stress $\left(\overline{u'w'}\right)$ and in fluxes of sensible heat, water vapour, and CO$_2$, ($\overline{w'T'}$, $\overline{w'q'}$, $\overline{w'c'}$, respectively) are written as follows:

$$d\overline{u'w'} = \overline{u'w'}\left(z + dz\right) - \overline{u'w'}(z) = -C_d u^2 df \tag{A.1}$$

$$d\overline{w'T'} = \overline{w'T'}\left(z + dz\right) - \overline{w'T'}(z) = C_h u\left(T_c - T\right) df \tag{A.2}$$

$$d\overline{w'q'} = \overline{w'q'}\left(z + dz\right) - \overline{w'q'}(z) = \left(C_{esl} df_{sl} + C_{esh} df_{sh}\right) u\Big[q_{SAT}\left(T_c - T\right)\Big] df \tag{A.3}$$

$$d\overline{w'c'} = \overline{w'c'}\left(z + dz\right) - \overline{w'c'}(z) = -\left(A_{sl} df_{sl} + A_{sh} df_{sh}\right) u \tag{A.4}$$

where C$_d$, C$_h$ and C$_e$ are the leaf transfer coefficients for momentum (both leaf surfaces), sensible heat (both leaf surfaces), and transpiration (lower leaf surface), respectively; u, w, T, q and c are the horizontal wind velocity (m s^{-1}), vertical wind velocity (m s^{-1}), air temperature, specific humidity and ambient CO$_2$ concentration, respectively. Where T_c and $q_{SAT}(T_c)$ are leaf temperature and saturated specific humidity at T_c, respectively; A the net assimilation rate per unit leaf area, df the leaf area index within a layer, and the subscripts sl and sh denote sunlit and shaded areas, respectively. C$_e$ is influenced by both the average stomatal conductance of the whole leaf (g_{sleaf}) and the boundary layer conductance (g_b) as follows:

$$C_e = \left(\frac{1}{g_b} + \frac{1}{g_{sleaf}}\right)^{-1} \frac{1}{u} \tag{A.5}$$

At the ground surface

$$\overline{u'w'}(0) = -C_{ds} u^2 \tag{A.6}$$

$$\overline{w'T'}(0) = C_{hs} u\left(T_s - T\right) \tag{A.7}$$

$$\overline{w'q'}(0) = \beta_{soil} C_{hs} u\left[q_{SAT}\left(T_s\right) - q\right] \tag{A.8}$$

where C$_{ds}$ and C$_{hs}$ are the bulk transfer coefficients at the soil surface for momentum and sensible heat, respectively; T_s and $q_{SAT}(T_s)$ are the soil surface temperature and saturated specific humidity at T_s, respectively; and b_{soil} is the moisture available at the ground surface. To calculate the fluxes at the ground surface, we used the wind velocity at dz (0.2 m in this study) from the soil surface. Assuming that C$_{hs}$ and C$_{ds}$ are similar, they are fixed as follows:

$$C_{hs} \approx C_{ds} = 0.015 \tag{A.9}$$

The soil respiration rate was used as a proxy for the flux of CO$_2$ at the ground surface.

When $q \le q_{SAT}(T_c)$, transpiration occurs from the dry part of the abaxial leaf surface, whereas evaporation occurs from the wet parts of the leaves.

$$d\overline{w'q'} = \left\{\left(C_{es1} df_{s1} + C_{esh} df_{sh}\right) \frac{df_{Ldry}}{df} + \left(\frac{C_h}{2}\right)\left(df_{Lwet} + df_{Uwet}\right)\right\} u\left(q_{SAT}\left(T_c\right) - q\right) \tag{A.10}$$

When $q > q_{SAT}(T_c)$, condensation occurred on both the adaxial and abaxial sides of the leaves.

$$d\overline{w'q'} = C_h u\left(q_{SAT}\left(T_c\right) - q\right) df \tag{A.11}$$

where q_{SAT} (T_c) is the saturated specific humidity at the leaf temperature and L, U, wet, and dry are the lower, upper, wet and dry temperatures, respectively.

The difference in CO$_2$ vapour flux between two layers in the canopy ($z + dz$ and z) is denoted as $d\overline{w'c'}$ (where w is the vertical wind velocity, and c is the specific humidity) can be written as follows:

$$d\overline{w'c'} = -\left(A_{sl}df_{sl} + A_{sh}df_{sh}\right)\frac{df_{Ldry}}{df}, \tag{A.12}$$

Sub-model (2): stomatal conductance and net photosynthesis for individual leaves

The net assimilation rate of individual leaves in each layer (A) was determined using a biochemical photosynthesis model (Farquhar et al. 1980), incorporating the values for stomatal conductance from the distribution of each patch:

$$A = V_c\left(1 - \frac{p\left(\Gamma_*\right)}{p\left(C_c\right)}\right) - R_{dleaf} \tag{A.13}$$

$$p\left(\Gamma_*\right) = \frac{p(O)}{2\tau} \tag{A.14}$$

where V_c is the rate of carboxylation in the photosynthetic carbon reduction cycle (mol m^{-2} s^{-1}), R_{dleaf} is the non-photorespiratory respiration rate (mol m^{-2} s^{-1}), p(G$*$) is the CO$_2$ compensation point without non-photorespiratory respiration (Pa), τ is the specificity factor of Rubisco, and $p(C_c)$ (Pa) and p(O) (21,000 Pa) are the partial pressures of CO$_2$ and O$_2$ at the sites of carboxylation and oxygenation, respectively. The lowest value between the electron transport-limited rate of carboxylation (W_j) and the RuBP saturated rate of carboxylation (W_c) was used as the velocity of carboxylation (Vc), as follows:

$$Wc = V_{cmax}\frac{p\left(C_c\right)}{p\left(C_c\right) + K_c\left(1 + \frac{p(O)}{K_o}\right)} \tag{A.15}$$

$$W_j = \frac{J}{4 + 8p\left(\Gamma_*\right)/p\left(C_c\right)} \tag{A.16}$$

where V_{cmax} is the maximum rate of carboxylation (mol m^{-2} s^{-1}), K_c and K_o are the Michaelis–Menten constants of rubisco for CO$_2$ and O$_2$, respectively, and J is the electron transport rate. J is expressed as the smaller root of the following nonrectangular hyperbola formula, representing the relationship with absorbed photosynthetically active radiation (Farquhar and Wong 1984).

$$\theta J^2 - \left[J_{max} + \frac{\varepsilon\left(1-f\right)}{2}Q\right]J + J_{max}\frac{\varepsilon\left(1-f\right)}{2}Q = 0 \tag{A.17}$$

In Eq. A.17, Q is the incident PAR (mol m^{-2} s^{-1}), e is the leaf absorbance of Q, f is the fraction of light lost not photosynthetically in the chloroplast lamellae, J_{max} is the maximum potential rate of electron transport and θ is a convexity factor. The values of θ (0.9) and $1 - f$ (0.85) were approximated using the results of the light curve measurements of the electron transport rate. The value of ε (0.7) was approximated by measuring the light penetration of the canopy leaves. Based on a study by Wullschleger (1993), J_{max} was related to V_{cmax} as follows:

$$J_{max} = k_j V_{cmax} \tag{A.18}$$

The Arrhenius function was used for the temperature dependence of the parameters K_c, Ko, t and $Rnleaf$ as follows:

$$f\left(T_{l,k}\right) = f\left(T_{ref}\right)\exp\left[\left(1 - \frac{T_{ref}}{T_{l,k}}\right)\frac{\Delta H_a}{RT_{ref}}\right] \tag{A.19}$$

A simplified equation from Sharpe and De Michele (1977) was used to determine the temperature dependence of V_{cmax} as follows:

$$f\left(T_{l.k}\right) = \frac{f\left(T_{ref}\right)\exp\left[\left(1 - \frac{T_{ref}}{T_{l,k}}\right)\frac{\Delta H_a}{RT_{ref}}\right]}{1 + \exp\left[\left(\Delta ST_{l,k} - \Delta H_d\right)/RT_{l.k}\right]} \tag{A.20}$$

where $f(T_{l.k})$ is the value of a given parameter at leaf temperature $T_{l.k}(K)$, $f(298)$ is the reference value of that parameter at 25.8 °C (K_{c25}, K_{o25}, $R_{dleaf25}$, τ_{25} and V_{cmax25}), ΔH_a is the activation energy (J mol^{-1}), ΔH_d is the deactivation energy (J mol^{-1}) and ΔS is an entropy term (J K^{-1} mol^{-1}). The determination of the rubisco kinetic parameters and their temperature dependencies remains a significant source of uncertainty (Dreyer et al. 2001). The values used in this study (Appendix 8) were primarily based on the work of Jordan and Ogren (1984), who used spinach, following Harley et al. (1992). R_{dleaf} was scaled using its relationship with the dark respiration rate (R_{nleaf}), based on the results of Brooks and Farquhar (1985), as follows:

$$R_{dleaf} = \begin{cases} R_{nleaf25} & for\ Q \le 5, \\ R_{nleaf25}\left[0.5 - 0.05\ln(Q)\right] & for\ Q \ge 5 \end{cases} \tag{A.21}$$

$R_{nleaf25}$ is related to V_{cmax} as follows:

$$R_{dleaf} = k_r V_{cmax} \tag{A.22}$$

The CO$_2$ concentration in the chloroplasts (C_c) was calculated under the assumption that this parameter equals the intercellular concentration of CO$_2$ as follows:

$$C_c = C_i = \frac{\left(g_{tc} - \frac{E}{2}\right)C_a - A}{g_{tc} + \frac{E}{2}} \tag{A.23}$$

$$\frac{1}{g_{tc}} = \frac{1}{g_{bc}} + \frac{1}{g_{sc}} \tag{A.24}$$

where C_a is the ambient CO$_2$ concentration (mol m^{-2} s^{-1}), C_i the intercellular CO$_2$ concentration (mol m^{-2} s^{-1}), E is the transpiration rate (mol m^{-2} s^{-1}) and g_{tc} is the total conductance of CO$_2$ (mol CO$_2$ m^{-2} s^{-1}). g_{bc} is the boundary layer conductance of CO$_2$ (mol CO$_2$ m^{-2} s^{-1}) such that g_{bc} = (g_{bw}/1.62)/3, and g_{sc} is the stomatal conductance of CO$_2$ (mol CO$_2$ m^{-2} s^{-1}) such that g_{sc} = g_{sw}/1.6, where g_{bw} is the boundary layer conductance of H$_2$O (mol H$_2$O m^{-2} s^{-1}), and g_{sw} is the stomatal conductance of H$_2$O (mol H$_2$O m^{-2} s^{-1}). Eq. A.23 incorporates the correction proposed by Jarman (1974) and von Caemmerer and Farquhar (1981) to account for the convective effects of transpiration through stomatal pores. The values of A and C_c were determined as the intersection points between the demand functions, as described by Eq. A.10 and the supply function described by Eq. A.23. An improved version of the model developed by Ball et al. (1987) and Leuning (1995) was used to estimate stomatal conductance, which is described as follows:

$$g_{sw} = m\frac{Af(D)}{C_s - \Gamma} + g_{swmin} \tag{A.25}$$

$$f(D) = \frac{1}{1 + \left(\frac{D}{D_0}\right)} \tag{A.26}$$

where f(D) is the non-linear function of the vapour pressure deficit, m the slope of the relationship between the stomatal index ($Af(D)/(C_s - \Gamma)$) and the stomatal conductance, C_s the CO$_2$ concentration at the leaf surface (mmol mol^{-1}), G the CO$_2$ compensation point (mmol mol^{-1}), and g_{swmin} is the minimum stomatal conductance. A hyperbolic form function similar to that of Lohammar et al. (1980) was used for $f(D)$, where D is the vapour pressure deficit (kPa) of air, and D_0 is the empirical value at which $f(D)$ halves. Leaf surface CO$_2$ concentration (C_s) was estimated using the chamber's air CO$_2$ concentration, constant boundary layer conductance, and net assimilation rate. The photosynthetic capacity was expected to decline exponentially with cumulative LAI as follows:

$$V_{cmax25}(\xi) = V_{cmax25}(0)\exp\left(-k_{V_c}\xi\right) \tag{A.27}$$

where ξ is the cumulative LAI measured downward from the top of the canopy and k_{Vc} is the extinction coefficient for $\mathrm{V}_{\mathrm{cmax25}}$.

Sub-model (3): radiative transfer within and above the canopy

The transfer of direct solar radiation ($S_{\mathrm{b}}\downarrow$) within a canopy is written as follows:

$$S_b\downarrow(z,H) = I_b S_b\downarrow\left(z+dz,H\right) \tag{A.28}$$

where I_{b} is the probability of no contact with direct radiation within a layer between z and $z + dz$ and H is the solar elevation. The transfer of direct PAR ($S_{\mathrm{PARb}}\downarrow$) within the canopy is analogous to (A.28). I_{b} is written as

$$I_b(H) = 1 - \frac{\Omega G_{layer}(H)df}{sinH} \tag{A.29}$$

The second term on the right is the shaded area of the foliage within a layer projected onto the horizontal plane. Ω is a clumping factor and ranges from 0 to 1. G_{layer} is the projected leaf surface area, accounting for leaf angle, which is the visible surface area assuming rainfall is vertical (Tanaka 2002). It indicates the ratio of the area of leaves 'in situ', projected into a plane normal to rainfall incident angle (H_p), which is assumed to be vertical. G_{layer} is the sum of G functions for each individual leaf within a layer (G_{leaf}). G_{leaf} is a function of solar elevation (H), leaf inclination angle (α), leaf orientation angle (β) and the direction of the sun (ϕ_s). G_{layer} can be represented by G_{leaf} and the distributions of the leaf inclination angle [g(α)] and leaf orientation angle [g(b)] within a layer. Assuming that the leaf orientation angle is constantly distributed [g(β)] = π/2], the direction of the sun can be ignored and G_{layer} can be written as follows:

$$G_{layer}(H) = \int_0^{2\pi}\frac{1}{2\pi}\int_0^{\frac{\pi}{2}} g(\alpha)\, G_{leaf}(\alpha,\beta,H)\, d\alpha d\beta \tag{A.30}$$

G_{leaf} is written as

$$G_{leaf}(\alpha,\beta,H) = |cos\alpha sinH + sin\alpha cos\beta cosH| \tag{A.31}$$

I_{d}, the probability of no contact with diffuse radiation within a layer between z and $z + dz$, was computed by integrating I_{b} over the sky hemisphere, if the diffuse solar radiation and PAR arrive uniformly from every angle of the sky hemisphere, as follows:

$$I_d = 2\int_0^{\pi/2} I_b(H) sinH cosH dH \tag{A.32}$$

Downward diffuse solar radiation ($S_{\mathrm{d}}\downarrow$) is written using I_{d}, leaf transmissivity (τ_{s}), and leaf reflectivity (ρ_{s}) as follows:

$$\begin{aligned} S_d\downarrow(z,H) = {} & S_d\downarrow\left(z+dz,H\right)\left[\tau_s\left(1-I_d\right)+I_d\right] \\ & +S_d\uparrow(z,H)\,\rho_s\left(1-I_d\right) \\ & +S_d\downarrow\left(z+dz,H\right)\tau_s\left(1-I_d\right) \end{aligned} \tag{A.33}$$

Upward diffuse solar radiation ($S_{\mathrm{d}}\uparrow$) is written as follows:

$$\begin{aligned} S_d\uparrow\left(z+dz,H\right) = {} & S_d\uparrow(z,H)\left[\tau_s\left(1-I_d\right)+I_d\right] \\ & +S_d\downarrow\left(z+dz,H\right)\rho_s\left(1-I_d\right) \\ & +S_b\downarrow\left(z+dz\right)\rho_s\left(1-I_b\right) \end{aligned} \tag{A.34}$$

The values of $S_{\mathrm{d}}\downarrow$ or $S_d\uparrow$ in the adjacent layers are required to solve Eqs A.33 and A.34, respectively. These values are initially unknown, but can be solved using the methods of Baldocchi and Hutchison (1986). Downward and upward diffuse PAR ($S_{\mathrm{PARd}}\downarrow$, $S_{\mathrm{PARd}}\uparrow$) are calculated by substituting PAR (τPAR, ρPAR) for leaf transmissivity (τ_{s}) and reflectivity (ρ_{s}) in Eqs A.33 and A.34. Solar radiation on the ground is expressed as follows:

$$S_d\uparrow(0) = \alpha_{S_{soil}}\left[S_b\downarrow(0) + S_b\uparrow(0)\right] \tag{A.35}$$

where α_{Ssoil} is the reflectivity of solar radiation on the ground. The PAR on the ground is obtained by substituting the reflectivity of the PAR on the ground ($\alpha_{PARsoil}$) for α_{Ssoil} in Eq. A.35. Downward long-wave radiation (L$\downarrow$) was calculated as follows:

$$L\downarrow(z) = L\downarrow\left(z+dz\right)I_d + \varepsilon_0\sigma T_c^4\left(1-I_d\right) \tag{A.36}$$

and upward long-wave radiation (L$\uparrow$) is calculated as follows:

$$L\uparrow\left(z+dz\right) = L\uparrow(z)I_d + \varepsilon_0\sigma T_c^4\left(1-I_d\right) \tag{A.37}$$

where ε_0 is the surface emissivity (1.0) and σ is the Stefan–Boltzmann constant (5.67×10^{-8} kg s^{-3} K^{-4}). The upward long-wave radiation on the ground is expressed as follows:

$$L\uparrow(0) = \varepsilon_0\sigma T_s^4 \tag{A.38}$$

A radiative transfer model is also required to evaluate the areas of sunlit and shaded leaves. The sunlit LAI (df_{su}) is expressed as follows:

$$df_{su} = \frac{S_b\downarrow\left(z+dz,H\right) - S_b\downarrow(z,H)}{S_b\downarrow\left(h,H\right)}\frac{sinH}{\Omega G_{layer}(H)} \tag{A.39}$$

where h is the canopy height and $S_{\mathrm{b}}\downarrow(h, H)$ is the direct solar radiation above the canopy. When $S_{\mathrm{b}}\downarrow(\mathrm{h, H}) = 0$ and df $df_{\mathrm{su}} = 0$, The shaded LAI (df_{sh}) is given by

$$\mathrm{df_{sh}} = \mathrm{df} - \mathrm{df_{su}} \tag{A.40}$$

The amount of PAR reaching the shaded part of the layer between z and $z + \mathrm{d}z$ (S_{PARsh}) is expressed as follows (Baldocchi and Hutchison 1986):

$$\mathrm{S_{PARsh}} = \mathrm{S_{PARd}}\uparrow\left(\mathrm{z+dz}\right) + \mathrm{S_{PARd}}\downarrow \tag{A.41}$$

Considering S_{PARsh} and direct PAR above the canopy (S_{PARb}(h, H)↓), the amount of PAR reaching the sunlit part of a layer (S_{PARsu}) is given (Baldocchi and Hutchison 1986):

$$S_{PARsu} = S_{PARsh} + S_{PARb} \downarrow (h, H) \frac{\Omega G_{layer}(H)}{sinH} \qquad (A.42)$$

According to the Bouguer and Berlage equations, the direct solar radiation and sky solar radiation at the top of the canopy on a clear day are expressed as follows:

$$S_b \downarrow = sinH \left(S_0 A_T^{\frac{1}{sinH}} \right) \qquad (A.43)$$

and

$$S_d \downarrow = 1.2 S_0 sinH \frac{(1 - A_T) \left(1 - A_T^{\frac{1}{sinH}} \right)}{(1 - 1.4 ln A_T)} \qquad (A.44)$$

where S_0 is the solar constant, A_T is atmospheric transmissivity, and H is solar elevation. The amount of global solar radiation is the sum of the sky and direct solar radiation.

Sub-model (4): leaf and ground surface energy balance

Ignoring both the heat storage in leaves and the energy stored by photosynthesis, the energy balance of leaves within a layer can be written as

$$(1 - \tau_s - \rho_s) \left\{ (I - I_b) S_b \downarrow (z + dz) + (1 - I_d) \right.$$
$$\left. [S_d \downarrow (z + dz) + S_d \uparrow (z)] \right\} + (1 - I_d) [L \downarrow (z + dz) + L \uparrow (z)]$$

$$= \lambda \rho_a d\overline{w'q'} + c_p \rho_a d\overline{w'T'} + 2\varepsilon_0 \sigma (T_c + 273)^4 (1 - I_d) \quad (A.45)$$

where λ is the latent heat of water vaporization, c_p is the specific heat of air at a constant pressure and ρ_{a} is the density of air.

The energy balance at the soil surface can be written as

$$(1 - \alpha_{sSoil}) [S_b \downarrow (0) + S_d \downarrow (0)] + L \downarrow (0) =$$

$$\lambda \rho_a \overline{w'q'}(0) + c_p \rho_a \overline{w'T'}(0) + \varepsilon_0 \sigma {T_s}^4 + G \qquad (A.46)$$

where G is the grand heat flux.

Sub-model (5): atmospheric diffusion within and above the canopy

A second-order closure model (Watanabe 1993) was used to describe the atmospheric diffusion within and above the canopy. The Reynolds stress, turbulent kinetic energy, variance of the vertical wind component, heat, water vapour and CO_2 fluxes are expressed as follows:

Reynolds stress $\left(\overline{u'w'}\right)$:

$$-\overline{w'^2} \frac{du}{dz} + 2 \frac{d}{dz} \left(e\lambda_1 \frac{d\overline{u'w'}}{dz} \right) - \frac{e}{3\lambda_2} \overline{u'w'} + \chi e^2 \frac{du}{dz} = 0 \qquad (A.47)$$

Turbulent energy (e^2):

$$-2\overline{u'w'} \frac{du}{dz} + \frac{d}{dz} \left[e\lambda_1 \left(\frac{de^2}{dz} + 2 \frac{d\overline{w'^2}}{dz} \right) \right] + 2C_d a u^3 - 2\frac{e^3}{\lambda^3} = 0 \qquad (A.48)$$

Variance of the vertical wind component $\left(\overline{w'^2}\right)$:

$$3 \frac{d}{dz} \left(e\lambda_1 \frac{d\overline{w'^2}}{dz} \right) - \frac{e}{3\lambda_2} \left(\overline{w'^2} - \frac{e^2}{3} \right) - \frac{2e^3}{3\lambda_3} = 0 \qquad (A.49)$$

Sensible heat flux $\left(\overline{w'T'}\right)$:

$$-\overline{w'^2} \frac{dT}{dz} + 2 \frac{d}{dz} \left(e\lambda_1 \frac{d\overline{w'T'}}{dz} \right) - \frac{e}{3\lambda_4} \overline{w'T'} = 0 \qquad (A.50)$$

Water vapour flux $\left(\overline{w'q'}\right)$:

$$-\overline{w'^2} \frac{dq}{dz} + 2 \frac{d}{dz} \left(e\lambda_1 \frac{dq'}{dz} \right) - \frac{e}{3\lambda_4} \overline{w'q'} = 0 \qquad (A.51)$$

CO_2 flux $\left(\overline{w'c'}\right)$:

$$-\overline{w'^2} \frac{dc}{dz} + 2 \frac{d}{dz} \left(e\lambda_1 \frac{dc'}{dz} \right) - \frac{e}{3\lambda_4} \overline{w'c'} = 0 \qquad (A.52)$$

where a is leaf area density, u' and w' are the fluctuations in the horizontal and vertical wind velocities, respectively, λ_{i}(i = 1–4) the length scale, e^2 twice the turbulent kinetic energy, and χ is a constant related to the energy redistribution. The length scale is expressed as

$$\lambda_i = \delta_i l \qquad (A.53)$$

where δ_i is a constant and l is the mixing length. Watanabe and Kondo (1990) described the maximum mixing length within and above the canopy (0 < z < h, h < z) and the mixing length at the canopy height (z = h) using the following equation, considering the limitation of the mixing length by both canopy elements and the ground surface:

$$l(z) \leq k \int_0^z \begin{matrix} \left\{ rexp \left[-\int_0^r \mu (z - t) dt \right] \mu (z - r \right\} dr \\ +kzexp \left[-\int_0^z \mu (z - t) dt \right] (0 < z < h, h < z) \end{matrix} \qquad (A.54)$$

$$\left| \frac{dl}{dk} \right| \leq k \qquad (z = h) \qquad (A.55)$$

$$l(h) = k \int_0^h \left\{ rexp \left[-\int_0^r \mu (h - t) dt \right] \mu (h - r) \right\} dr$$
$$+ khexp \left[-\int_0^h \mu (h - t) dt \right] \qquad (A.56)$$

$$\mu(z) = \frac{C_d a(z)}{2k^2} \qquad (A.57)$$

where r is the distance from the point at z to a lower point z to a lower point 0 ≤ r ≤ z. The value of δ_1 was 0.23 based on the work of Mellor and Yamada (1974), and the values of χ (=0.077), δ_2(=0.85), δ_3 (=16.6) and δ_4 (=0.567) were determined using the following boundary conditions above the canopy (h ≤ z; Watanabe 1993):

$$\overline{w'x'} = -u_* x_* \qquad (A.58)$$

$$\frac{dx}{dz} = \frac{x_*}{l} \qquad (A.59)$$

$$\frac{de}{dz} = \frac{d\overline{w'^2}}{dz} = \frac{d\overline{w'x'}}{dz} = 0 \qquad (A.60)$$

where x corresponds to u, T, q and c; u_*, T_*, q_* and c_* are the friction velocity, temperature, specific humidity and CO_2 concentration, respectively.

Following Wilson and Shaw (1977), the boundary conditions at twice the canopy height can be written as

$$\frac{e^2}{{u_*}^2} = 6.5 \tag{A.61}$$

$$\frac{\overline{w\prime^2}}{{u_*}^2} = 1.5 \tag{A.62}$$

Sub-model (6): interception of rainfall and the leaf water budget

The sub-model of interception and leaf water budget was based on the rainfall interception model proposed by Watanabe and Mizutani (1996). Model 1 used the same sub-models of rainfall interception and leaf water budget applied by Kosugi et al. (2006), Takanashi et al. (2003) and Tanaka (2002). Leaf water storage in the vertical profile was estimated as follows:

$$W = W_L + W_U \tag{A.63}$$

where W_L and W_U are the water storage on the lower (abaxial) and upper (adaxial) surfaces of the leaves per leaf area, respectively.

The wet leaf area index on the upper sides is estimated as

$$df_{Uwet} = r_{wetu} W_U / W_{UMAX} df \tag{A.64}$$

where, r_{wetu} is maximum abaxial wet leaf area fraction by interception on the upper side. In all 4 models, r_{wetu} was equal to 1, indicating that the entire adaxial surface of the leaves received interception.

In Models 1, 3 and 4, the leaf area index on the lower side was estimated as

$$df_{Lwet} = r_{wetL} W_L / W_{LMAX} df \tag{A.65}$$

where r_{wetL} is the maximum abaxial wet leaf area fraction by interception on the lower side of the plant. In Models 1, 3 and 4, r_{wetL} is equal to 1. In Model 2, r_{wetL} was equal to 0.5. Notably, Model 1 did not receive interception from the abaxial side of the leaf, and the only source of abaxial leaf wetness was condensation (Eqs A.66, A.69). Because the probability and amount of condensation were small, the abaxial surface of Model 1 often remained dry, even though its r_{wetL} was equal to 1. For Models 2, 3, and four, the abaxial side of the leaf received interception (Eqs A.66, A.69); therefore, the entire abaxial surface of the leaf can be wetted by interception in Models 4 and 3, and half of the abaxial surface of the leaf can be wetted by interception in Model 2. W_{UMAX} and W_{LMAX} are the water storage capacities of the upper and lower leaf surfaces, respectively. When df equals 1, df_{Lwet} in Eq. A.65 represents the simulated abaxial wet area fraction (Fig. 7). The values of W_U/W_{UMAX} and $W_L/\mathrm{W_{LMAX}}$ are the ratios of the wet area to the entire area of the upper and lower leaf surfaces, respectively, at a given height within the canopy.

Correspondingly, the dry leaf area index of each surface is estimated as

$$df_{dry} = df - df_{wet} = \left(1 - \frac{W}{W_{max}}\right) df \tag{A.66}$$

The change in the amount of water stored on the leaf surface during a very short time can be described as the ratios of the change in the water budget of leaves (∂W) to time (∂t) as follows using precipitation (P), evaporation, or condensation rate per unit area on one side (E_p) and G_{layer}.

When $q \leq q_{SAT}(T_c)$, rainfall with a canopy layer is

$$P(z) = \left\{1 - \frac{G_{layer}(H_p)}{\sin H_p P} df_{Udry}\right\} P(z + dz) \tag{A.67}$$

For all four models, the ratios of change in the water budget on the adaxial side of the leaves were expressed as follows:

$$\frac{\partial W_U}{\partial t} = \frac{G_{layer}(H_P)}{\sin(H_P)} \left(1 - \frac{W_U}{W_{UMAX}}\right) P - E_p \left(\frac{W_U}{W_{UMAX}}\right) \tag{A.68}$$

The ratio of the change in the water budget on the abaxial side of the leaves was expressed as follows:

$$\frac{\partial W_L}{\partial t} = P_L \frac{G_{layer}(H_P)}{\sin(H_P)} \left(1 - \frac{W_L}{W_{LMAX}}\right) P - E_p \left(\frac{W_L}{W_{LMAX}}\right) \tag{A.69}$$

where P_L denotes the absolute interception capacity. $P_\mathrm{L} = 0$ indicates that the abaxial side of the leaf cannot intercept rainfall (Model 1), $P_\mathrm{L} = 1$ indicates that the abaxial side of the leaf can intercept rainfall (Models 2, 3 and 4).

When $q > q_{SAT}(T_c)$, rainfall with a canopy layer is

$$P(z) = \left\{1 - \frac{G_{layer}(H_p)}{\sin H_p P} df_{Udry}\right\} P(z + dz) - E_p \left(df_{Uwet} + df_{Lwet}\right) \tag{A.70}$$

For all models, the ratios of change in the water budget on the adaxial side of the leaves were written as

$$\frac{\partial W_U}{\partial t} = \left\{\frac{G_{layer}(H_P)}{\sin(H_P)} P - E_p\right\} \left(1 - \frac{W_U}{W_{UMAX}}\right) \tag{A.71}$$

The ratio of the change in the water budget on the abaxial side of the leaves was expressed as follows:

$$\frac{\partial W_L}{\partial t} = \left\{P_L \frac{G_{layer}(H_P)}{\sin(H_P)} P - E_p\right\} \left(1 - \frac{W_L}{W_{LMAX}}\right) \tag{A.72}$$

For Model 1, P_L equals 0; for Model 2, 3 and 4, P_L equals 1.

Sub-model (7): soil respiration

The Q_{10} function was applied to evaluate the soil respiration rate in the original multilayer model as follows:

$$\overline{w'c'}(0) = F_{REsoil} = F_{REsoil15} Q_{10soil}^{\left(\frac{T_s - 15}{10}\right)} \tag{A.73}$$

where F_REsoil is the flux from the soil (mg m^{-2} s^{-1}), T_s soil temperature at a reference depth (2 cm), F_REsoil15 (mg m^{-2} s^{-1}) is the F_REsoil at a soil temperature of 15 °C at the reference depth, and Q_{10soil} is the Q_{10} value for the temperature dependence in soil respiration rate.

Parameters used in the estimation of CO_2 fluxes in the SVAT multilayer model

Parameter	Symbol	Value	Unit	Reference
Measurement height		29	m	This study
Canopy structure				
Canopy height		20	m	This study
Leaf area index		4.9	$m^2\ m^{-2}$	This study
Leaf inclination		35.5		Takanashi et al. 2003
Leaf area density distribution	p,q	16, 2.2		This study
Clumping factor	Ω	1		Tsuruta et al. 2016
Leaf optical characteristics				
Transmissivity of solar radiation and PAR	τ	0.2, 0.06		Ross 1975
Reflectivity of solar radiation and PAR	ρ	0.15, 0.09		Takanashi et al. 2003
Leaf physical characteristics				
Drag coefficient on both leaf surfaces	C_d	0.2		Wilson and Shaw 1977
Bulk transfer coefficient for sensible heat on both leaf surfaces	C_b	0.09		Takanashi et al. 2003
Water storage capacity on both surfaces (Model 1, 2, 3)	W_{umax}	0.18	mm per unit leaf area	This study
Soil physical and optical characteristics				
Drag coefficient on soil surface	C_{ds}	0.015		Takanashi et al. 2003
Bulk transfer coefficient for sensible heat on soil surface	C_{bs}	0.015		Takanashi et al. 2003
Moisture availability	β_{soil}	0.2		Takanashi et al. 2003
Reflectivity of solar radiation and PAR	α_{soil}	0.26, 0.064		Takanashi et al. 2003
Referential soil respiration rate at 15 °C	F_{Resoil}	2.7	$\mu mol\ m^{-2}\ s^{-1}$	This study
Q_{10} value of soil respiration rate	Q_{10soil}	2.19		This study
Leaf gas exchange characteristics				
Stomatal coefficient	m	6		Tsuruta et al. 2016
Minimum stomatal conductance	g_{smin}	0.005	$mol\ m^{-2}\ s^{-1}$	This study
V_{cmax} at 25 °C	V_{cmax25}	40	$\mu mol\ m^{-2}\ s^{-1}$	This study
Activation energy for V_{cmax}	$\Delta H_a(V_{cmax})$	56,900	$J\ mol^{-1}$	This study
Deactivation energy for V_{camx}	$\Delta H_d(V_{cmax})$	199,500	$J\ mol^{-1}$	This study
Entropy term	$\Delta S(V_{cmax})$	650	$J\ K^{-1}\ mol^{-1}$	This study
Extinction coefficient for V_{cmax25}	k_{Vc}	0.7		Kosugi et al. 2006
Proportion of Rnleaf25 to V_{cmax25}	k_r	0.034		Kosugi et al. 2006
Activation energy for R_{dleaf}	$\Delta H_a(R_{dleaf})$	52,000	$J\ mol^{-1}$	This study
Proportion of J_{max} to V_{cmax}	k_j	2.1		Kosugi et al. 2006
Convexity factor	θ	0.9		This study
Leaf absorbance of Q	ε	0.7		This study
Fraction of light loss not used photosynthetically at the chloroplast lamellae	$1-f$	0.85		This study
K_c at 25 °C	K_{c25}	27.5	Pa CO_2	Harley and Baldocchi 1995
Activation energy for K_c	$\Delta H_a\ (K_c)$	80,470	$J\ mol^{-1}$	Harley et al. 1992
K_o at 25 °C	K_{o25}	42,000	Pa O_2	Harley and Baldocchi 1995
Activation energy for K_o	$\Delta H_a\ (K_o)$	14,510	$J\ mol^{-1}$	Harley et al. 1992
τ at 25 °C	τ_{25}	2321		Harley and Baldocchi 1995
Activation energy for τ	$\Delta H_a\ (\tau)$	−29,000	$J\ mol^{-1}$	Harley and Baldocchi 1995

Sensitivity test for key parameters

A brief sensitivity analysis was conducted; this step was necessitated by the fact that most of the parameters applied in this model were obtained from a dry canopy. The results of the NEE simulation (Fig. 6) were compared using distinctive parameters. Three key parameters of rainfall interception and leaf photosynthesis calculations were tested.

Stomatal coefficient

The stomatal coefficient (m) (Leuning 1995; Kosugi and Matsuo 2006) reflects the influence of soil water content on stomatal conductance in an improved ball-type stomatal conductance model (Eq. A.25). The value of m is largely species-dependent. Considering the possible improvement of stomatal conductance after rainfall, we estimated NEE when m was 9 and 12 (i.e. greater than the used value, corresponding to a larger stomatal conductance) according to the m range reported by Leuning (1995) as in Figs A.9.1 and A.9.2. The average NEE for the four models with different m at wet time is shown in Table A.9.1. CO_2 uptake increased along with the improvement of stomatal conductance. The results showed that NEE simulation is a little sensitive to the variation of m. However, the four models remain the similar gaps

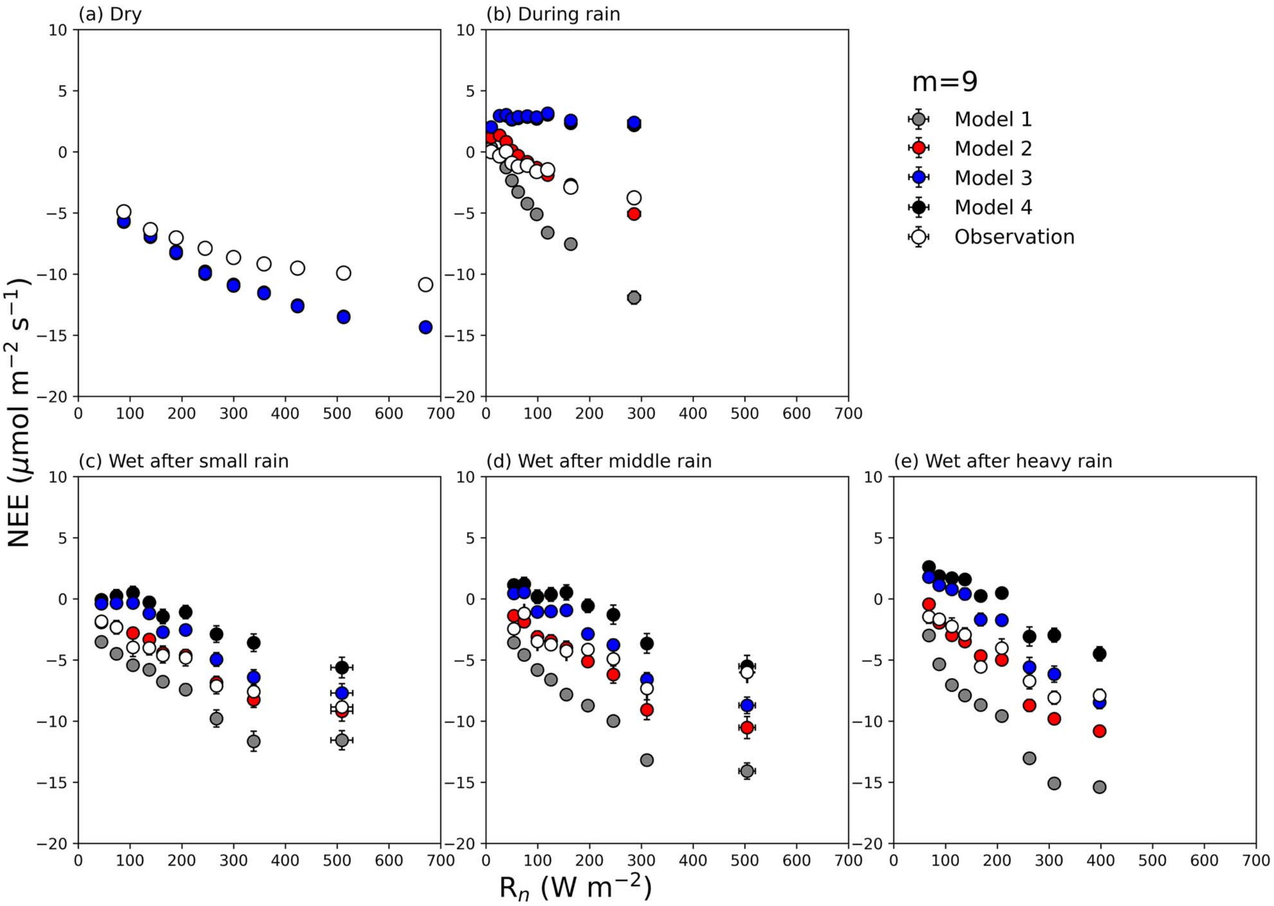

Figure A.9.1. NEE of different periods during and after rainfall, corresponding to Fig. 6 when the stomatal coefficient (*m*) was 9.

Table A.9.1. Average simulated NEE (μmol m^{-2} s^{-1}) from the four models with varied stomatal coefficient (*m*) during the wet time.

m	6.00	9.00	12.00
Model 1	−5.87	−6.24	−6.36
Model 2	−3.00	−3.21	−3.29
Model 3	−0.42	−0.54	−0.61
Model 4	0.48	0.36	0.30

Table A.9.2. Average simulated NEE (μmol m^{-2} s^{-1}) from the four models with varied bulk transfer coefficient for sensible heat on both leaf surfaces (C_h) during the wet time.

C_h	0.06	0.09	1.00
Model 1	−5.78	−5.87	−5.79
Model 2	−2.88	−3.00	−2.93
Model 3	−0.35	−0.42	−0.11
Model 4	0.49	0.48	0.21

Table A.9.3. Average simulated NEE (μmol m^{-2} s^{-1}) from the four models with varied water storage capacity of the upper leaf surface (W_{Umax}, mm per unit leaf area) during the wet time.

W_{Umax}	0.15	0.18	0.2
Model 1	−5.78	−5.87	−5.80
Model 2	−3.03	−3.00	−2.87
Model 3	−0.63	−0.42	−0.35
Model 4	0.26	0.48	0.60

like Fig. 6 when *m* was increased though the values were fluctuated.

Bulk transfer coefficient for sensible heat on both leaf surfaces

The bulk transfer coefficient for sensible heat on both leaf surfaces (C_h) plays a crucial role in the determination of the leaf water budget and the interception transfer among the leaf layers (Eqs A.10, A.11). We assessed the NEE under two different C_h values as 0.06 (lower than the used value of 0.09) and 0.1 (i.e. higher than the used value), as shown in Figs A.9.3 and A.9.4, respectively. Although there were slight variations in the NEE values across all four models with different C_h values (Table A.9.2), similar discrepancies between these models and the observed NEE are shown in Figs A.9.3, A.9.4 and Fig. 6. Also, Models 1 and 2 showed similar average NEE with varied C_h value, but Models 3 and 4 (the two models have the whole abaxial surface to receive interception) show a response to the varied C_h value. This indicates the sensitivity of the simulated NEE to C_h is slight and will not influence the differences in CO_2 uptake among these models. This result corresponds to the insensitivity of the interception amounts to C_h change reported by Komatsu et al. (2008).

Water storage capacity of the upper leaf surface

The water storage capacity of the upper leaf surface (W_{Umax}, Eqs A.64, A.68, A.71) is obtained by leaf wetness

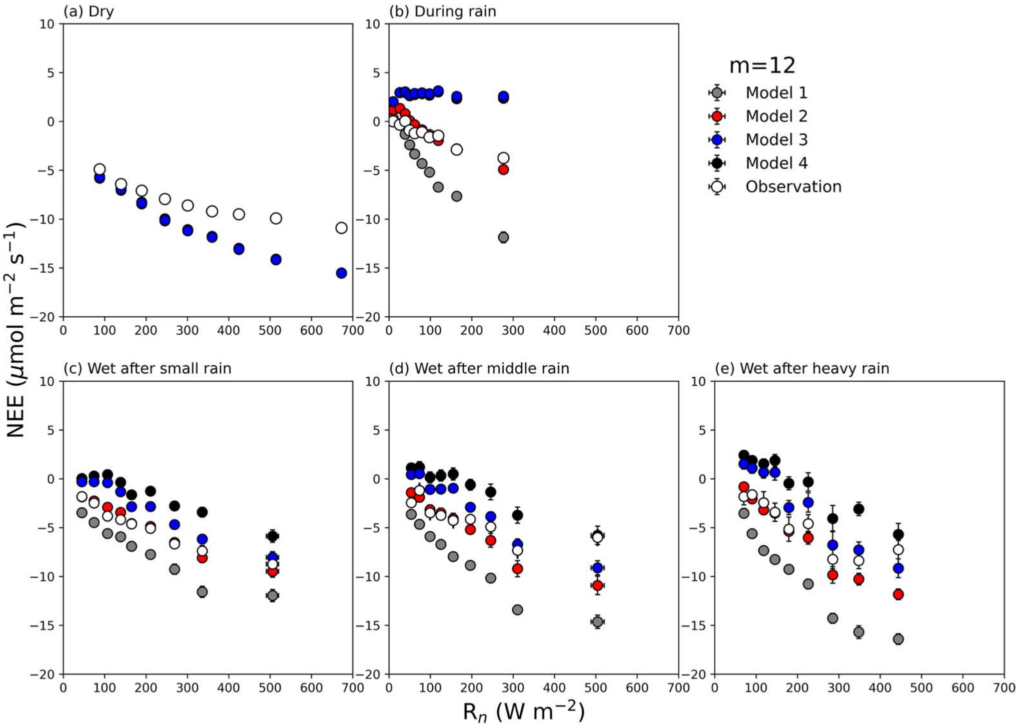

Figure A.9.2. NEE of different periods during and after rainfall, corresponding to Fig. 6 when stomatal coefficient (m) was 12.

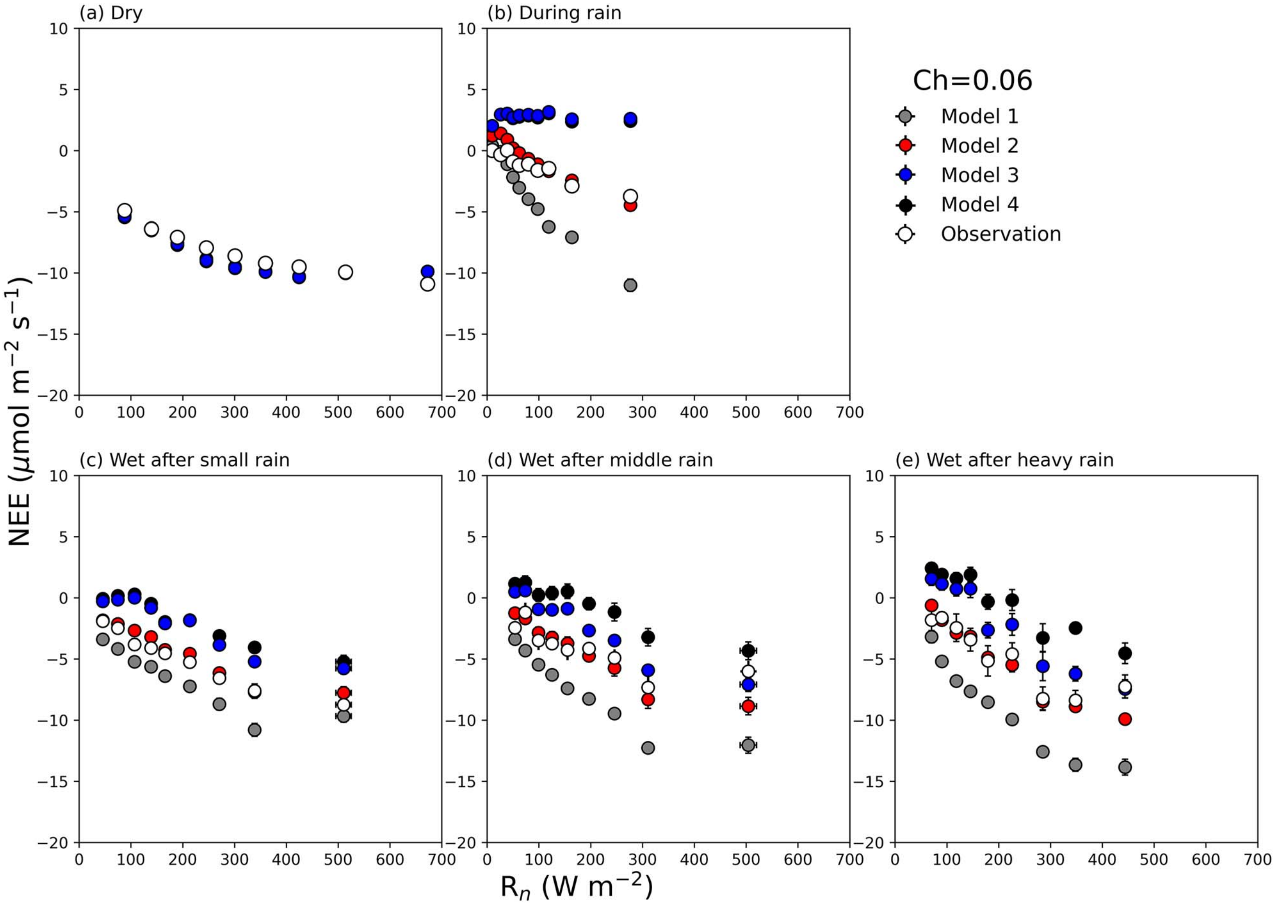

Figure A.9.3. NEE of different periods during and after rainfall, corresponding to Fig. 6 when bulk transfer coefficient for sensible heat on both leaf surfaces (C_h) was 0.06.

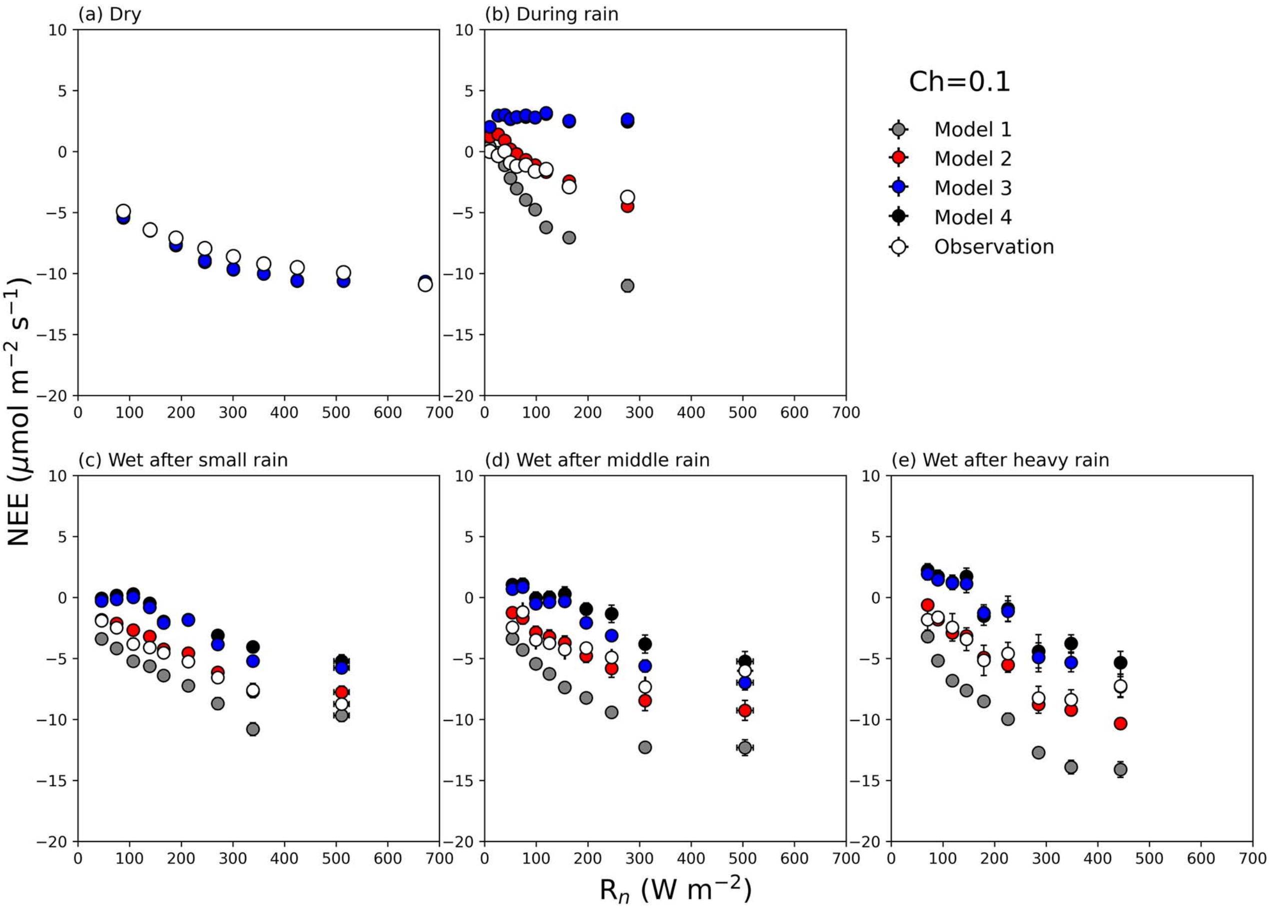

Figure A.9.4. NEE of different periods during and after rainfall, corresponding to Fig. 6 when bulk transfer coefficient for sensible heat on both leaf surfaces (C_h) was 0.1.

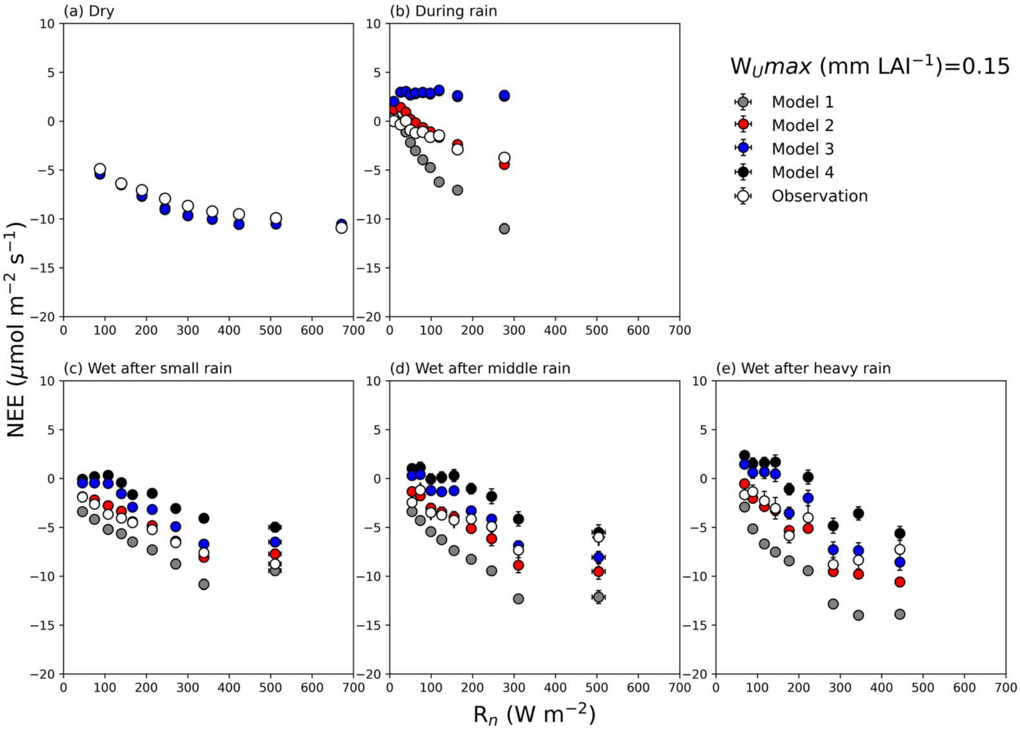

Figure A.9.5. NEE of different periods during and after rainfall, corresponding to Fig. 6 when water storage capacity of the upper leaf surface (W_{Umax}) was 0.15 mm per leaf area.

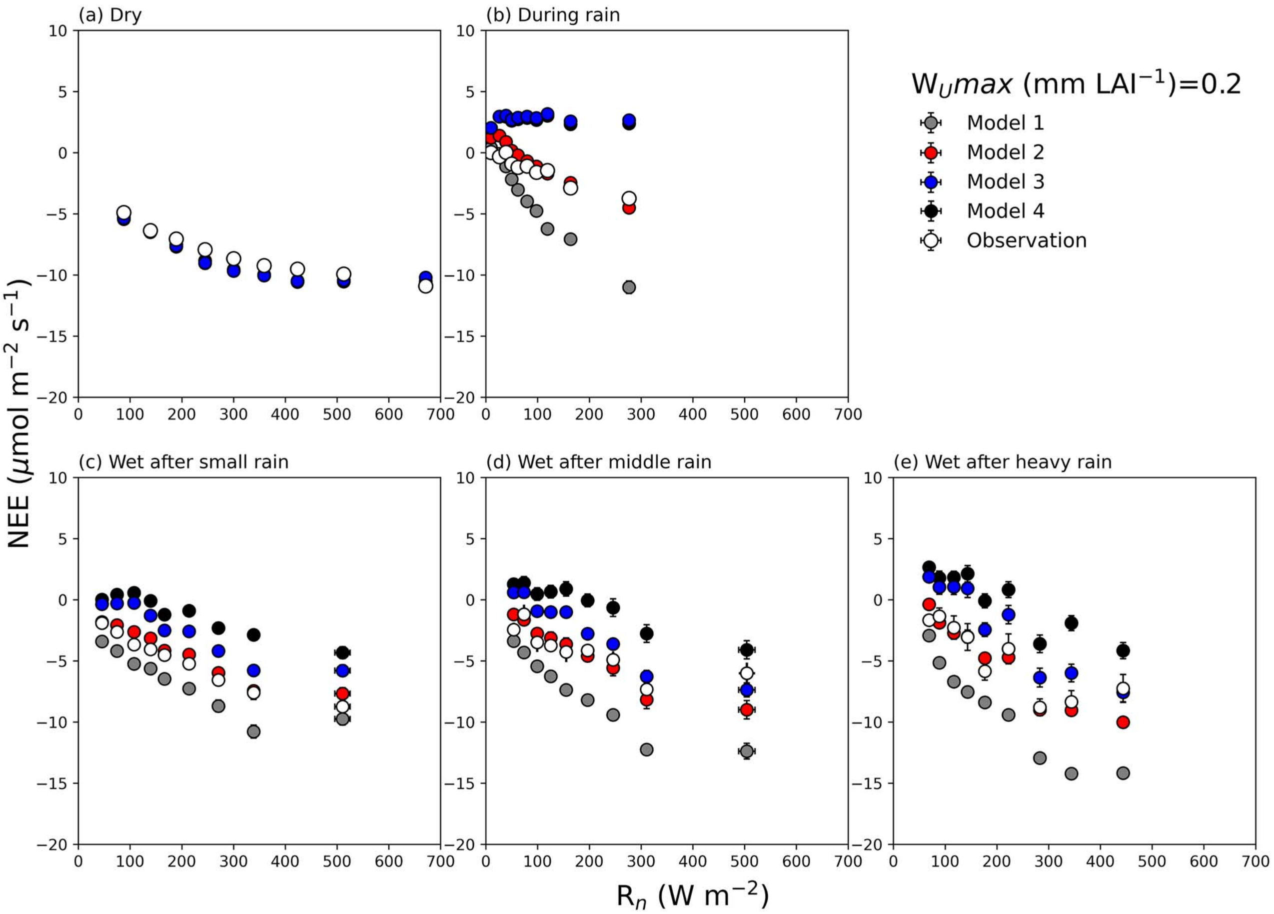

Figure A.9.6. NEE of different periods during and after rainfall, corresponding to Fig. 6 when water storage capacity of the upper leaf surface (W_{Umax}) was 0.2 mm per leaf area.

experiment (Jiao et al. 2022). We estimated the NEE when W_{Umax} was 0.15 (i.e. less than the value of 0.18) and 0.2 (i.e. greater than the used value) W_{Umax} range reported by Takanashi et al. (2003) as in Figs A.9.5 and A.9.6. The change in W_{Umax} had the largest influence on Model 2 after rainfall (c), (d), and (e) in Figs A.9.5, A.9.6 and Fig. 6. The wet canopy NEE of the 4 models changed when W_{Umax} varied. This indicated that W_{Umax} is an important parameter for evaluating wet-canopy photosynthesis. In addition, the influence of a lower surface water storage capacity on wet canopy photosynthesis was analysed by comparing Models 1, 3 and 4. The change of W_{Umax} led to little difference for Models 1 and 2 NEE, but the average NEE in wet time for Models 3 and 4 changed apparently (Table A.9.3). This means the value of W_{Umax} is more significant for the situation that whole abaxial surfaces receive interception.